

Diffuse Axion Background

Joshua Eby^{a,b} and Volodymyr Takhistov^{c,d,e,b}

^a*The Oskar Klein Centre, Department of Physics, Stockholm University, 10691 Stockholm, Sweden*

^b*Kavli Institute for the Physics and Mathematics of the Universe (WPI), Chiba 277-8583, Japan*

^c*International Center for Quantum-field Measurement Systems for Studies of the Universe and Particles (QUP, WPI), High Energy Accelerator Research Organization (KEK), Oho 1-1, Tsukuba, Ibaraki 305-0801, Japan*

^d*Theory Center, Institute of Particle and Nuclear Studies (IPNS), High Energy Accelerator Research Organization (KEK), Tsukuba 305-0801, Japan*

^e*Graduate University for Advanced Studies (SOKENDAI), 1-1 Oho, Tsukuba, Ibaraki 305-0801, Japan*

E-mail: joshua.eby@fysik.su.se, vtakhist@post.kek.jp

Abstract: Relativistic axions can be readily produced in a broad variety of transient sources, such as axion star bosenova explosions, supernovae or even evaporating primordial black holes. We develop a general framework describing the resulting persistent diffuse axion background (DaB) due to accumulated axions from historic transient events. We derive strong constraints on the DaB flux from light axions $m \lesssim 10^{-3}$ eV emitted from sources with energies $\omega \gtrsim$ MeV considering the non-observation of excess photons associated with axion-photon coupling from experiments, including COMPTEL, NuSTAR, XMM-Newton, INTEGRAL, EGRET and Fermi. Future searches in experiments such as SKA, JWST, XRISM, Vera C. Rubin Observatory, AMEGO/e-ASTROGAM will allow probing DaB and associated axion-photon couplings with unprecedented sensitivity covering a wide range of possible source energies as low as $0.1 \mu\text{eV}$ and multiple decades in axion masses. We highlight the differences between astrophysical and dark sector sources of DaB. Further, we discuss complementarity with direct detection as well as prospects for other DaB searches. Our analysis demonstrates that DaB can act as a promising probe of populations of axion emission sources as well as emission mechanisms.

Contents

1	Introduction	2
2	Diffuse axion background flux	3
2.1	Cosmological transient event rate	5
2.2	Emission sources	7
2.2.1	Supernovae	8
2.2.2	Axion star bosonovae	9
2.2.3	Primordial black hole evaporation	11
2.2.4	Main-sequence stellar emission	11
2.2.5	Neutron stars	12
2.2.6	Examples of other sources	13
2.3	Comparison to local DM flux	14
3	Axion conversion to photons	16
3.1	Magnetic fields	17
3.2	Axion decay	19
4	Observable signatures with photons	21
4.1	Limits from X-ray and gamma-ray searches	22
4.2	Sensitivity of future searches	25
5	Case study: axion star bosonovae	29
6	Complementary search prospects	32
6.1	Axion-electron and other couplings	32
6.2	Direct detection	34
7	Conclusions	35
	Acknowledgments	36
A	Results for different cosmological rate functions	36
B	Photon flux estimates for future experiments	39
	Bibliography	56

1 Introduction

The discovery of Higgs boson [1, 2] has highlighted the central role of scalar spin-0 particles in Nature. Existence of pseudo-scalar spin-0 quantum chromodynamics (QCD) axions would readily address the long-standing strong CP problem of the Standard Model (SM) [3–9] and provide a compelling candidate for the dark matter (DM) [10–12]. Axions and more generally axion-like particles¹, pseudo-scalars that generically arise from broken shift symmetries, are expected to be ubiquitous from fundamental theory [13, 14]. Significant efforts have been devoted to explore the axion landscape (see e.g. [15–17] for an overview), primarily focusing on non-relativistic cold axion DM.

Relativistic axions can appear from a variety of sources. Cosmological axion production at redshifts prior to galaxy and star formation ($z \gtrsim 30$) will result in new contributions to the cosmic axion background [18–20]. Another prominent possibility are thermal axions, which are produced in the early Universe if axions were in thermal equilibrium through interactions with SM constituents [20–27]. Efficient non-thermal cosmological axion production is also possible, such as due to particle decays [28–31] or non-linear dynamics of field oscillations [32–34]. On the other hand, continuous emission at low-redshifts of relativistic axions from astrophysical sources like stars and the Sun has resulted in variety of sensitive tests of possible axion parameter space, such as by considerations of star cooling [35] or direct detection searches for solar axion emission [36, 37].

Recently, a fruitful new direction focusing on manifestations of relativistic burst axion emissions from transient sources has emerged and is being explored, including axion (boson) star explosions [38, 39], black hole superradiance [40–45], and solar halos [46–48] that can repeatedly explode on astrophysical timescales. Direct detection of relativistic bosons emitted from transient sources was found to result in a rich variety of signatures in the context of axion searches [49, 50] as well as precision quantum sensors [51], often allowing to probe novel parameter space that is beyond the reach of conventional cold DM searches. Furthermore, such axion manifestations hold promising avenues for exploration of new physics in the context of multimessenger astronomy [49, 51, 52].

Accumulation of relativistic axions from historic transient sources will result in persistent axion flux filling the Universe [53–56]. We comprehensively explore this *diffuse axion background* (DaB). An analogy can be drawn between DaB and neutrinos emitted from historic astrophysical sources, such as supernovae, which will contribute to a diffuse supernova neutrino background (see e.g. [57] for review), detection of which is a target of ongoing efforts by Super-Kamiokande [58, 59] and other neutrino experiments, or other possible sources such as supermassive star explosions [60–62]. Proposed searches for axions contributing to cosmic axion background, e.g. [63–68], could also be in principle considered for diffuse axion background.

In this work, we develop a general framework and systematically analyze DaB originating from distinct sources. Depending on the origin, DaB contributions can dramatically differ.

¹Here, we denote axion and axion-like particles as *axions*.

We discuss variety of general approaches for DaB detection, including with existing as well as future experiments.

The format of this paper is as follows. In Sec. 2 we introduce the general framework for DaB and discuss different possible contributing sources. In Sec. 3 we focus on photon production from DaB . Then, in Sec. 4 we analyze observable signatures with photons originating from DaB for different existing as well as future experiments. Later, in Sec. 5 we focus on analyzing DaB associated with axion star bosonovae emission as a characteristic source example. We discuss other DaB search prospects in Sec. 6, including different axion couplings as well as direct detection. We conclude in Sec. 7.

2 Diffuse axion background flux

The present-day accumulated DaB number flux spectrum that originates from historic transient sources can be stated in generality in analogy with the well-studied diffuse background flux of SM weakly interacting neutrinos originating from sources like historic core-collapse supernovae [57, 69] (or e.g. supermassive star explosions [60, 62, 70]) as²

$$\frac{d\phi}{d\omega} = \int_0^\infty dz(1+z) \frac{dN_a(\omega(1+z))}{d\omega} R_{\text{burst}}(z) \left| \frac{dt}{dz} \right|, \quad (2.1)$$

where ω is the axion energy, $R_{\text{burst}}(z)$ is the rate density of transient “burst” events emitting axions due to a particular source (in units of events per time and per volume) as a function of cosmological redshift z , and $dN_a/d\omega$ is the differential spectrum of the number of axions N_a per unit energy ω characterizing emitted axions from a single transient burst with the $(1+z)$ factor accounting for the energy redshifting of axions emitted at $z > 0$. The last term encodes the cosmology of flat expanding Universe dominated by matter and cosmological constant $|dt/dz|^{-1} = H_0(1+z)\sqrt{\Omega_\Lambda + \Omega_M(1+z)^3}$, with $H_0 = 67.4 \text{ km s}^{-1} \text{ Mpc}^{-1}$, and densities $\Omega_\Lambda = 0.685$ for cosmological constant and $\Omega_M = 0.315$ for matter compatible with latest measurements from Planck [71]. The flux for various possible sources, including both astrophysical as well as dark-sector sources, is illustrated in Fig. 1.

Looking ahead, relevant for DaB detection are axion interactions with SM, which generally depend on specific theory. More so, for astrophysical transient sources, axion-SM interactions are also generally responsible for their production as energy is converted from SM constituents to axions. A canonical coupling of pseudoscalar axion a is the two-photon coupling described by the Lagrangian contribution

$$\mathcal{L} \supset \frac{1}{4} g_{a\gamma} a F_{\mu\nu} \tilde{F}^{\mu\nu} = g_{a\gamma} a \mathbf{E} \cdot \mathbf{B}, \quad (2.2)$$

where $F_{\mu\nu}$ is the electromagnetic field-strength tensor, $\tilde{F}^{\mu\nu}$ is its dual, and $g_{a\gamma}$ the axion-photon coupling³. Interacting with external magnetic field \mathbf{B} , the coupling of Eq. (2.2)

²The conventional units for emission spectrum ϕ are $\text{cm}^{-2}\text{s}^{-1}$.

³This coupling has typical dimension of GeV^{-1} .

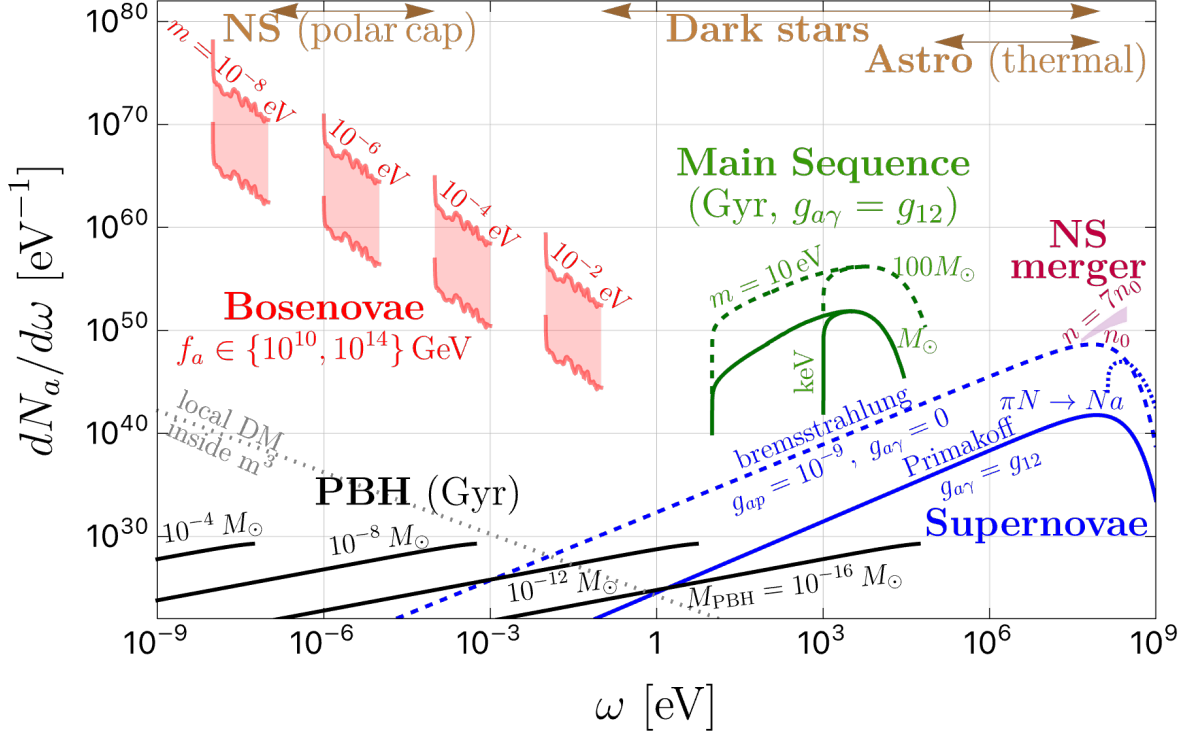


Figure 1: Sources of relativistic axion flux emission, which can contribute to the DaB as described in Sec. 2.2. **Blue:** Supernova (SN) emission estimated from Ref. [54] (blue dashed corresponding to bremsstrahlung with axion proton coupling $g_{ap} = 10^{-9}$, $g_{a\gamma} = 0$ allowed by constraints from excessive SN cooling [72], axion-photon coupling, blue solid for Primakoff processes with $g_{a\gamma} = g_{12} \equiv 10^{-12} \text{ GeV}^{-1}$, and $\pi N \rightarrow Na$ production using $g_{ap} = 10^{-9}$ [73, 74]). **Red:** Axion star bosenova emission estimated from numerical simulations of Ref. [39] (shaded region corresponds to axion decay constant between $f_a = 10^{14} \text{ GeV}$, top, and $f_a = 10^{10} \text{ GeV}$, bottom). **Black:** Primordial black hole (PBH) emission through Hawking radiation (emission timescale $\Delta t = \text{Gyr}$, PBH mass $M_{\text{PBH}} \in \{10^{-4}, 10^{-8}, 10^{-12}, 10^{-16}\} M_{\odot}$, assuming $m \ll \omega$). **Green:** Stellar emission from Main Sequence stars [75] (solid and dashed lines correspond to stellar masses of M_{\odot} and $100M_{\odot}$, respectively, fixing $\Delta t = \text{Gyr}$ and $g_{a\gamma} = g_{12}$). **Purple:** Neutron star (NS) merger emission estimated from Ref. [76, 77] (with the energy fixed by the temperature as $\omega/3 = T = (20 - 100) \text{ MeV}$, density between $n = (1 - 7)n_0$, and neutron coupling fixed to $g_{an} = 1.5 \times 10^{-9}$). **Brown:** Expected energy range for NS polar cap emission, astrophysical thermal emission, and dark star thermal emission are denoted by arrows. Reference flux from the local DM density inside an experimental volume of m^3 is given by the gray dotted line.

results in axion-photon conversion that is a prominent source of phenomenological signatures. Additional possible axion interactions include

$$\mathcal{L} \supset \frac{g_{a\chi}}{2m_{\chi}} \partial_{\mu} a \bar{\chi} \gamma^{\mu} \gamma_5 \chi + \frac{g_{ag}}{4} a G_{\mu\nu} \tilde{G}^{\mu\nu}, \quad (2.3)$$

where $G_{\mu\nu}$ is the gluon field strength tensor, $\tilde{G}_{\mu\nu}$ is its dual, χ denotes fermions such as nucleons N (protons, neutrons) or electrons e , m_χ is their mass, and $g_{a\chi}$ and g_{ag} are coupling constants. For QCD axion that resolves the CP problem in the SM QCD sector, the axion mass m and couplings are related to the Peccei-Quinn symmetry breaking scale, also called the axion decay constant, f_a . In particular, $(m/1 \text{ eV}) = (7 \times 10^6 \text{ GeV}/f_a) = 0.5\xi g_{a\gamma}/(10^{-10} \text{ GeV}^{-1})$ with ξ being a model-dependent constant, which in KSVZ QCD axion scenario [6, 7] is $|\xi| \simeq 0.5$ and in DFSZ QCD axion scenario [8, 9] is $|\xi| \simeq 1.4$.

2.1 Cosmological transient event rate

To capture a broad class of possible DaB sources, it is convenient to parameterize the cosmological transient event rate as

$$R_{\text{burst}}(z) = \frac{A\rho_{\text{loss}}H_0}{E_{\text{tot}}(z)} f(z), \quad (2.4)$$

where $f(z)$ is a dimensionless function of redshift z characterizing transient source distribution. Here, the normalization constant A is fixed by the requirement that the energy density ρ_{loss} in axions emitted from a particular transient source type, such as exploding axion stars, constitutes a specified subdominant fraction of the total DM density⁴

$$\rho_{\text{loss}} = \int dt E_{\text{tot}}(z) \frac{R_{\text{burst}}(z)}{(1+z)^3} = \frac{1}{H_0} \int dz \frac{E_{\text{tot}}(z) R_{\text{burst}}(z)}{(1+z)^4 \sqrt{\Omega_\Lambda + \Omega_M(1+z)^3}}, \quad (2.5)$$

where $E_{\text{tot}}(z)$ is the total energy emitted in each transient event burst at redshift z . Since for the sources we consider the total emitted energy for each event is predominantly independent of redshift, we take E_{tot} to be constant in what follows. We can set the normalization constant A by inverting Eq. (2.5) as

$$A = \left[\int dz' \frac{f(z')}{(1+z')^4 \sqrt{\Omega_\Lambda + \Omega_M(1+z')^3}} \right]^{-1}, \quad (2.6)$$

which can be directly computed for a given source model $f(z)$. In general, $f(z)$ could have non-vanishing contributions over the redshift range $z \in \{z_{\text{min}}, z_{\text{max}}\}$, where z_{max} is the redshift when explosive transient axion emission events begin to occur and z_{min} when the transient events subside. We consider $z_{\text{min}} \rightarrow 0$, although theories of transient axion sources with non-negligible z_{min} can be readily incorporated in our analysis.

The energy density ρ_{loss} can be intuitively expressed as the fraction \mathcal{F} of the average DM energy density in the Universe, $\rho_{\text{DM}} \simeq 1.2 \times 10^{-6} \text{ GeV}/\text{cm}^3$, as $\rho_{\text{loss}} = \mathcal{F}\rho_{\text{DM}}$. We consider $\mathcal{F} = 0.1$ as a reference benchmark, which can evade various constraints. As we will show below, some of our signatures are detectable even for significantly smaller DM fractions.

⁴In case of exploding supermassive stars, analogous normalization can be imposed by considering relation with baryon abundance [62].

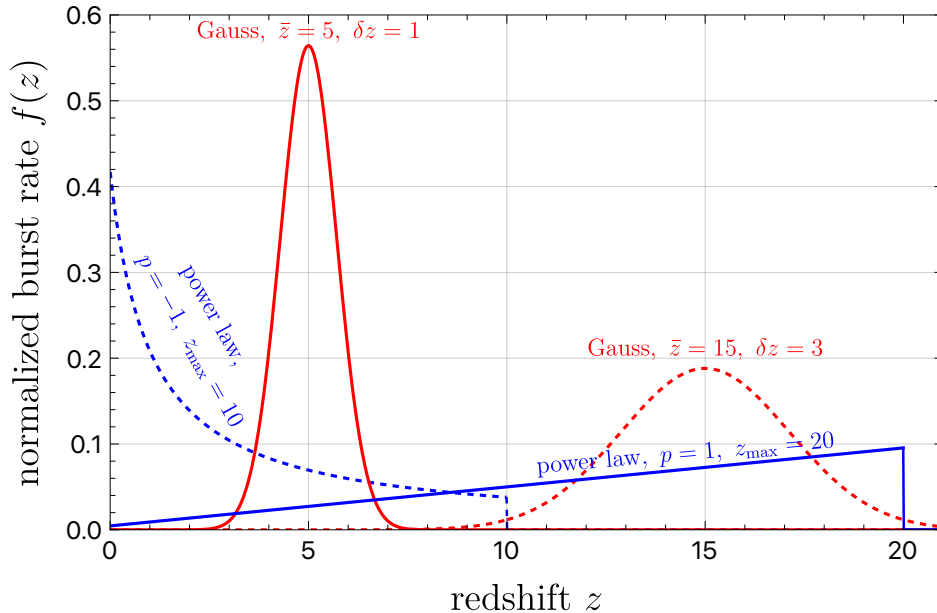


Figure 2: Dimensionless cosmological transient axion burst event rate distribution $f(z)$ sourcing relativistic axions that are considered in this work. The power-law and Gauss distributions are defined in Eq. (2.7), and we set the input parameters as labeled. For illustration we normalize $f(z)$ to unity.

The cosmological event rate $R_{\text{burst}}(z)$ characterizes the epochs during which the transient sources are most active. Employing the normalization of Eq. (2.4), we analyze two characteristic phenomenological models of source events, described by

$$f(z) = \begin{cases} (1+z)^p \Theta(z - z_{\text{max}}) & \text{power law} \\ \exp[-(z - \bar{z})^2 / \delta z^2] & \text{Gauss.} \end{cases}, \quad (2.7)$$

where p is an integer, and \bar{z} with δz denote the Gaussian distribution mean and width, respectively. The power law is motivated by scenarios where the transient source rate is smoothly varying with possible additional redshift dependence as specified by parameter p , reaching a maximum in the present-day for $p < 0$ or at earlier times for $p > 0$. The Gaussian model instead characterizes general scenarios where transient events predominantly occur during a relatively short cosmological epoch, which could be associated with some dynamical processes, with a duration approximated by $z \in \{\bar{z} - \delta z, \bar{z} + \delta z\}$. We illustrate several distributions considered in this work in Fig. 2. Our analysis can readily be carried over to other choices of source event rates, specific to particular theories.

With $f(z)$ given by Eq. (2.7), we can directly compute normalization A of Eq. (2.6). For

the power-law model we find

$$A_1 = \left[\int_0^{z_{\max}} dz' \frac{(1+z')^{p-4} \Theta(z-z_{\max})}{\sqrt{\Omega_\Lambda + \Omega_M(1+z')^3}} \right]^{-1} \simeq \frac{1}{\sqrt{\Omega_M}} \left(\frac{9}{2} - p \right) + \mathcal{O}(z_{\max}^{p-9/2}), \quad (2.8)$$

which is valid as long as $p < 9/2$, and where we approximated $\sqrt{\Omega_\Lambda + \Omega_M(1+z)^3} \simeq \sqrt{\Omega_M(1+z)^3}$ considering Universe is matter-dominated for the majority of redshift values of interest⁵. Further corrections are suppressed by powers of $1/z_{\max}$, which we consider to be subdominant compared to unity. For the Gaussian distribution

$$A_2 = \left[\int_0^{z_{\max}} dz' \frac{\exp\left(-\left(\frac{z'-\bar{z}}{\delta z}\right)^2\right)}{(1+z')^4 \sqrt{\Omega_\Lambda + \Omega_M(1+z')^3}} \right]^{-1}. \quad (2.9)$$

Evaluating Eq. (2.9) numerically, one finds $A_2 \simeq 1 - 10^6$ upon varying $\delta z \simeq 10^{-2} - 1$ and $\bar{z} \simeq 0 - 20$. In this estimate we used $z_{\max} = 20$, but the results do not depend significantly on this choice as long as $z_{\max} > \bar{z}$ is satisfied. In what follows, we focus on the power-law model for simplicity and outline results for the Gaussian model in App. A.

2.2 Emission sources

The flux of axions in the relativistic background, given in Eq. (2.1), depends sensitively on the spectrum of emission from transient sources $dN_a/d\omega$. Our general analysis framework can be applied to a wide range of possible transient sources. A generic description of a peaked axion burst can be captured by a Gaussian function

$$\left. \frac{dN_a(\omega)}{d\omega} \right|_{\text{Gauss}} = C \frac{E_{\text{tot}}}{m^2} \frac{\exp\left(-\left(\frac{\omega-\bar{\omega}}{\delta\omega}\right)^2\right)}{\sqrt{\pi}(\delta\omega/m)}, \quad (2.10)$$

with a central peak energy $\bar{\omega}$ and a width $\delta\omega$. The normalization of the emission spectrum $m \int d\omega (dN_a/d\omega) = E_{\text{tot}}$ implies that the normalization constant is given by

$$C = m \left[\int \frac{\exp\left(-\left(\frac{\omega-\bar{\omega}}{\delta\omega}\right)^2\right)}{\sqrt{\pi}(\delta\omega/m)} d\omega \right]^{-1} = 2 \left[1 + \text{erf}\left(\frac{\bar{\omega}}{\delta\omega}\right) \right]^{-1}. \quad (2.11)$$

Note that C is independent of m and E_{tot} .

We can employ the Gaussian function description to determine the axion background density for a generalized emission source, considering the emission follows an approximately peaked structure. In the limit $\delta\omega \rightarrow 0$, $(dN_a/d\omega)_{\text{Gauss}} \rightarrow (CE_{\text{tot}}/m)\delta(\omega - \bar{\omega})$, capturing the effect of a narrow burst spectrum in the $\delta\omega \ll m$ limit. Combining Eqs. (2.1), (2.4), (2.10),

⁵Corrections induced by this approximation are of order $\mathcal{O}(1)$ at most.

and (2.11), we obtain

$$\left. \frac{d\phi}{d\omega} \right|_{\text{Gauss}} = \frac{\mathcal{F}\rho_{\text{DM}}}{m\delta\omega} \frac{2}{\sqrt{\pi}} \frac{A}{[1 + \text{erf}(\bar{\omega}/\delta\omega)]} \int \frac{dz f(z)}{\sqrt{\Omega_{\Lambda} + \Omega_M(1+z)^3}} \exp \left[- \left(\frac{(\omega(1+z) - \bar{\omega})}{\delta\omega} \right)^2 \right]. \quad (2.12)$$

We stress that the flux model of Eq. (2.12) captures key behavior while being particularly straightforward to analyze. For a given particle mass m and cosmological rate function $f(z)$, one needs only to specify the central burst energy $\bar{\omega}$, the emission width $\delta\omega$, and the total DM fraction converted to relativistic particles \mathcal{F} .

We systematically discuss below several prominent examples of transient axion burst sources resulting in DaB highlighting the generality and reach of our analysis. In Fig. 1 we summarize axion emission flux from several characteristic sources, as compared to reference local DM flux within a volume of m^3 (see Eq. (2.25)). Analogously to astrophysical multi-messenger targets, astrophysical sources such as supernovae can serve as prime production sites of relativistic axions⁶. This exemplifies conversion of energy associated with SM constituents (e.g. baryons) into dark sectors with large kinetic energy. In this work, in addition to astrophysical sources, we emphasize the significant potential of dark-sector dynamics to produce relativistic axions resulting in sizable contributions to DaB, which we can describe using a general and flexible framework. We further illustrate how this can give rise to photon signatures across a broad variety of source classes, range of energy scales, and distinct photon-production scenarios.

2.2.1 Supernovae

Astrophysical sources could serve as powerful production sites not only of neutrinos, but also of other weakly interacting particles such as axions. Core-collapse supernovae (SN) allow to sensitively probe axions through variety of methods (e.g. [35, 78–81]). Aside first direct SN neutrino observations [82–84], SN1987A that exploded in the Large Magellanic Cloud at a distance of 50 kpc proved to be an essential laboratory for axion physics (e.g. [78, 85–91]). In SN, efficient axion production can occur through axion nucleon-nucleon bremsstrahlung process [85] $NN \rightarrow NN a$, where N denotes nucleons (protons, neutrons). Refs. [73, 74] have illustrated the importance of a pion production channel $\pi N \rightarrow N a$ as well, which can dominate axion emission above energies of order ~ 150 MeV. Requiring that SN1987A neutrino emission is not significantly reduced by axion emission, we consider axion-nucleon coupling⁷ $g_{aN} \lesssim 10^{-9}$ [72]. When axions couple only to photons with coupling $g_{a\gamma}$, efficient production can occur through Primakoff process when thermal photons are converted into axions within electromagnetic field of stellar medium [92]. This results in strong limits on axions from SN energy loss arguments more stringent than other limits above tens of keV [93–96]. For light SN axions constraints arise from conversion to photons in Milky Way Galactic

⁶We note that some astrophysical axion emission mechanisms can persist over significant timescales. Here, we comment on them as characteristic and reference sources in the context of potentially contributing to DaB.

⁷Exact value depends on specific considered axion model.

magnetic field [97–99]. For heavy SN axions constraints arise from decays along the emitted axion line of sight and non-observation of SN1987A coincidence signal [100].

Contributions to DaB from SN [53–55] can be effectively parameterized using a fit to the axion spectrum arising due to a given process channel x of the form [54]

$$\left. \frac{dN_a(\omega)}{d\omega} \right|_{\text{supernova}} = c \left(\frac{g_{ax}}{g_{ax}^{\text{ref}}} \right)^2 \left(\frac{\omega}{\omega_0} \right)^\beta \exp \left(-\frac{(\beta+1)\omega}{\omega_0} \right), \quad (2.13)$$

where c , g_{ax}^{ref} , ω_0 , and β are fit parameters which depend on the production process (see e.g. Tab. 1 of Ref. [54]). Hypernovae, transient sources similar to supernovae but with higher energy and which give rise to a black hole in the final state, are also efficient sources of axions, with a spectrum that peaks around $dN_a/d\omega \sim 10^{44}/\text{eV}$ per second (for $g_{a\gamma} \simeq 10^{-12} \text{ GeV}^{-1}$) between 10 – 100 MeV [101].

Importantly, for astrophysical transients such as SN contributing to DaB the event rate R_{burst} is determined by conventional astrophysical processes (e.g. star formation, stellar nuclear fusion) such as in case of diffuse neutrino background. However, this is distinct for DaB contributions arising from dark sector transient sources such as axion stars explosions.

2.2.2 Axion star bosenovae

Axion stars are gravitationally-bound states formed from ultralight bosons [102–105]. They can appear in the early Universe within the in cores of diffuse axion miniclusters [106, 107]. When their mass reaches a critical value M_c [108–112], defined by the strength of the axion self-interaction coupling, these states undergo gravitational collapse and finally emit a large fraction of their mass-energy in relativistic bosons [38, 39]. This explosive production of relativistic particles signifies⁸ *bosenova*.

Detailed numerical simulations of boson star collapse and explosive axion emission were carried out in Ref. [39]. The spectrum of emitted axions dE/dk has been analyzed up to $k/m \simeq 9$, where $E(\omega) = \omega N_a(\omega)$ is the total energy emitted in axions of energy ω , and $k = \sqrt{\omega^2 - m^2}$ is the corresponding momentum. The total energy emitted is a linear function of the axion decay constant f_a , well-fitted by $E_{\text{tot}} \simeq M_c [0.3 + 10^3 f_a / M_{\text{Pl}}]$, which saturates to unity near $f_a \simeq 10^{16} \text{ GeV}$, and where $M_c = 10 M_{\text{Pl}} f_a / m$. To analyze resulting DaB flux using Eq. (2.1), we translate

$$\left. \frac{dN_a(\omega)}{d\omega} \right|_{\text{bosenova}} = \left[\frac{dE}{dk} - \frac{d\omega}{dk} \right] \frac{1}{\omega \frac{d\omega}{dk}} \simeq \frac{dE}{dk} \frac{1}{\sqrt{\omega^2 - m^2}}, \quad (2.14)$$

where in the last step we used $d\omega/dk = k/\omega$, and neglected the second term in the bracket, which is suppressed by a factor $1/N_a \ll 1$ relative to the leading term. In this case, Eqs. (2.1)

⁸The term was originally coined to describe an explosive process in atomic physics [113].

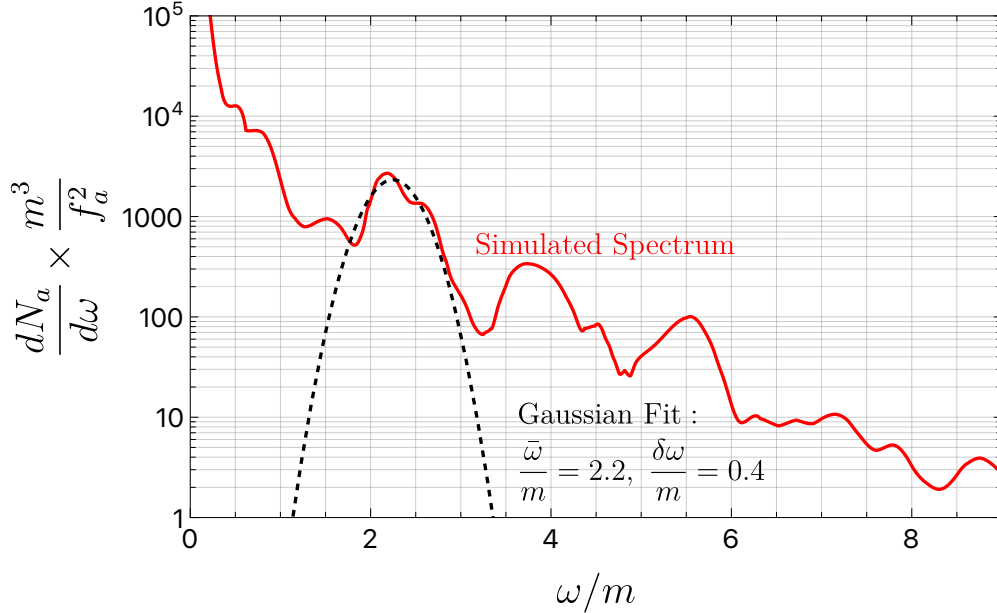


Figure 3: Spectrum of emitted axions as a function of energy, from numerical simulations of axion bosenova explosion [39] (red solid) with a Gaussian fit (black dashed) using Eq. (2.10) to the leading relativistic peak at $\bar{\omega} \simeq 2.2m$ and $\delta\omega \simeq 0.4m$.

and (2.4) give

$$\left. \frac{d\phi}{d\omega} \right|_{\text{bosenova}} \simeq \frac{\mathcal{F}\rho_{\text{DMA}}}{\sqrt{\omega^2 - m^2}} \int_0^\infty dz \frac{f(z)}{\sqrt{\Omega_\Lambda + \Omega_M(1+z)^3}} \frac{1}{E_{\text{tot}}} \frac{dE(\omega(1+z))}{dk}. \quad (2.15)$$

Key properties of these axion star explosions can be obtained from the emission spectrum [39], which is peaked at semi-relativistic energies (i.e. momenta of order $\sim \text{few} \times m$). The peaks can be understood as a consequence of number-changing processes (see e.g. Ref. [114, 115]). In Fig. 3 we illustrate the full simulated spectrum of Ref. [39], along with a Gaussian fit of the first relativistic peak, which is well-described by Eq. (2.10) with $\bar{\omega} \simeq 2.2m$ and $\delta\omega \simeq 0.4$ as shown. Explosive bosenova emissions across astrophysical timescales constitute a prominent contribution to DaB arising from dark-sector sources.

Recently, our analyses of direct detection signatures from bosenova explosions occurring inside the Milky Way demonstrated that they constitute particularly promising targets for current and near-future experimental searches [49, 51]. Ref. [116, 117] suggested that repeated mergers of DM subhalos can give rise to a large abundance of near-critical boson stars, obtaining a DM fraction as large as $\sim 10^{-6}$. These stars would collapse at redshift $z \lesssim 30$, with the resulting relativistic axions contributing to DaB . Bosenovae occurring at earlier epochs of redshifts $z \gtrsim 30$ can also contribute, albeit with significantly redshifted axion energies, and can be constrained by cosmological observations [118].

2.2.3 Primordial black hole evaporation

Relativistic axions can be readily emitted as Hawking radiation when the black hole temperature exceeds the axion mass from evaporating primordial black holes (PBHs), which can form in the early Universe through variety of mechanisms, providing a novel target for direct searches [119–123]. The emission rate of axions produced in Hawking radiation per unit energy per unit time is given by [124–126]

$$\frac{d^2 N_a}{d\omega dt} = \frac{1}{2\pi} \frac{\Gamma(m, \omega, M_{\text{PBH}})}{e^{\omega/T_{\text{H}}} - 1}, \quad (2.16)$$

where $T_{\text{H}} = (8\pi GM_{\text{PBH}})^{-1} = 1.06 (10^{13} \text{ g}/M_{\text{PBH}}) \text{ GeV}$ is the Hawking temperature. The greybody factor Γ can be computed numerically in general (see e.g. [127, 128]), but can be approximated with the geometric-optics limit for high-energy emission as $\Gamma \simeq 27G^2 M_{\text{PBH}}^2 \omega^2$. In that limit, we can write

$$\left. \frac{dN_a}{d\omega} \right|_{\text{PBH}} \simeq \frac{27\Delta t}{2\pi} \frac{(GM_{\text{PBH}}\omega)^2}{e^{8\pi GM_{\text{PBH}}\omega} - 1} \simeq \frac{27\Delta t}{16\pi^2} GM_{\text{PBH}}\omega, \quad (2.17)$$

where Δt is the total emission time and in the second step we expanded considering $\omega \ll T_{\text{H}}$. In addition to contributing to the DaB, the emitted axions can be promptly converted to photons. In Fig. 1 we illustrate the flux of axions from PBH evaporation assuming $\Delta t = \text{Gyr}$ and that $m \ll \omega$. Recently, it was shown that intriguing electromagnetic signatures can also appear from decays of sterile neutrinos originating from evaporating PBHs [129, 130].

Note that Eq. (2.17) assumes the PBH mass does not change appreciably due to emission, which is a good approximation for $M_{\text{PBH}} \gtrsim 10^{-16} M_{\odot}$. In this limit PBHs act as an approximately continuous source of axion production, though transient signatures are possible during the final stages of PBH evaporation.

2.2.4 Main-sequence stellar emission

Stars can continuously emit axions, primarily through Primakoff effect and photon coalescence. The emission peak for such axions is near energies of the order of the star’s core temperatures, typically $\bar{\omega} \sim \text{keV}$ for stellar masses $(0.1 - 100)M_{\odot}$. The luminosity L_a^* of such sources was computed in detail in Ref. [75] for stars in this mass range, which can be converted to a particle flux using

$$\left. \frac{dN_a}{d\omega}(\omega) \right|_{\text{stars}} = \frac{dL_a^*}{d\omega} \frac{\Delta t}{\omega}, \quad (2.18)$$

with Δt being the total emission time. In Fig. 1 we illustrate the flux considering $\Delta t = \text{Gyr}$ and Primakoff production, which is the dominant contribution for the majority of the parameter space of interest. This continuous stellar axion emission can readily contribute to DaB, as has been recently studied in Ref. [75]. Beyond main-sequence stars, post-main-sequence

and population III stars could also potentially source axions and contribute to DaB with sufficient core temperatures.

2.2.5 Neutron stars

Neutron stars (NSs) constitute another possible prominent astrophysical source of relativistic axion emission. Axions can be thermally produced inside NSs through various channels, such as nucleon-nucleon bremsstrahlung $NN \rightarrow NNa$ and Cooper pair-breaking processes, cooling NSs⁹ (e.g. [135–137]). Additional production modes are possible in highly-magnetized NSs, i.e. magnetars [138]. Such emission can be enhanced during NS mergers, a process which has been studied using numerical [139] and analytic [76, 77] approaches. The typical energy scale of emission is near the temperature of a NS $T \simeq \mathcal{O}(1 - 100)$ MeV, provided the axions are massless by comparison, i.e. $m \ll T$. Furthermore, for typical nuclear couplings allowed by current constraints (see e.g. [17] for review), the axions easily escape the star and free-stream away.

The axion emissivity in NS mergers as a function of temperature, $Q_0(T)$, has been estimated in relativistic mean field theory [76] for an axion-neutron coupling of $g_0 = 1.5 \times 10^{-9}$. For other couplings, the emissivity scales as

$$Q(T) = \left(\frac{g_{an}}{g_0}\right)^2 Q_0(T). \quad (2.19)$$

Following Ref. [76], we use the temperature T as a proxy for the typical axion emission energy as $\omega \simeq 3T$. Taking an approximate merger duration of $t_{\text{merger}} \sim 1$ s and emitting volume of $V \sim (15 \text{ km})^3$ [77], we estimate

$$\left.\frac{dN_a}{d\omega}\right|_{\text{NS merger}} \simeq \frac{V t_{\text{merger}}}{\omega^2} Q(T). \quad (2.20)$$

Here, the density of the Fermi fluid n is varied between the nuclear saturation density, $n_0 \simeq 10^{-44} \text{ m}^3$, and $7n_0$. This range determines the extent of the gray shaded region in Fig. 1. Some of the emitted axions convert to gamma rays in the magnetosphere, leading to detectable, transient photon signals [77]. Here, we consider the possibility of such axions accumulating over time and contributing to DaB. Other axion emission signatures from neutron star mergers are also possible, for example, in the case of fireball formation [140, 141].

Recently, it was pointed out that axions can be produced directly via a coupling to photons in the polar-cap region of NS [142, 143]. While some become trapped around the NS, for axions with masses $m \lesssim 10^{-7}$ eV the vast majority escape the NS (as many as $\sim 10^{50}$ axions per second), as the energy scale of emission is fixed by dynamics in the polar cap in the range $10^{-7} \text{ eV} \lesssim \omega \lesssim 10^{-4} \text{ eV}$ [144]. As we discuss further below, such frequency ranges could be probed with future Square Kilometer Array (SKA) observations.

⁹Cooling of white dwarfs and red giants through axion emission can also result in sensitive constraints [131–134].

2.2.6 Examples of other sources

A broad variety of other sources of relativistic axion emission that could contribute to DaB are possible, such as:

- **Black hole superradiance:** “clouds” of axions can be generated by sapping the angular momentum and energy from rapidly-rotating black holes [40–44, 145] (see e.g. [146] for review). Superradiance effects around early-Universe (primordial) black holes have also been considered [45, 147, 148]. Massive axion fields that have quasi-bound states around black holes with $\omega < l\Omega_H$, where Ω_H is the angular velocity of the black hole horizon¹⁰ and l is the angular momentum around the black hole spin axis, can experience exponentially unstable growth. The timescale for spin-down of the BH is give by [43]

$$\tau_{\text{spin-down}} \simeq 10^7 \text{ years} \left(\frac{0.02}{r_S m}\right)^5 \left(\frac{10^{-12} \text{ eV}}{m}\right) \left(\frac{0.9}{a_*}\right)^{3/2} \left(\frac{10^{15} \text{ GeV}}{f_a}\right)^2. \quad (2.21)$$

The growth continues until the black hole loses most of its angular momentum or the superradiance is quenched by the axion self-interactions, either by exciting axions out of superradiant modes leading to stable steady-state configuration or by inducing gravitational collapse. In the latter case, an explosive bosonova-like event occurs near the black hole with rapid emission of relativistic axions [40]. Axion emission can be modified in case of binary black hole mergers [149]. We note that the event rates of bosonovae-type events associated with black hole superradiance sensitively depends on a variety of factors such as black hole population statistics, distributions of black hole masses and spins, as well as particle physics effects like interaction couplings of the axions.

- **Stellar axion halos:** axions can be captured directly in the gravitational field of astrophysical bodies, such as stars. These configurations are akin to gravitational atoms, having a spherically-symmetric density profile of the form [46, 47]

$$\rho(r, t) \simeq \rho_0(t) \exp\left(-\frac{r^2}{R_*^2}\right), \quad (2.22)$$

with radius R_* and central density $\rho_0(t)$ which can grow exponentially in magnitude with time [48]. Gravitational collapse of these structures around stars across galaxies can potentially lead to occurrence of yet another class of bosonova-like explosive events. The rate of growth happens on a timescales similar to the known relaxation timescales

¹⁰Here, $\Omega_H = \frac{1}{r_S} \left(\frac{a_*}{1+\sqrt{1-a_*^2}}\right)$, where $r_S = 2GM_{\text{BH}}$ is the black hole Schwarzschild radius and $a_* = J/GM_{\text{BH}}^2$ is the dimensionless spin of black hole with angular momentum J .

for ultralight particles¹¹ [48], which for $2 \rightarrow 2$ self-interactions takes the form

$$\tau_{\text{rel}} \simeq \frac{64 f_a^4 m^3 v_{\text{IDM}}^2}{\rho_{\text{IDM}}^2} \simeq 9 \text{ Gyr} \left(\frac{f_a}{10^8 \text{ GeV}} \right)^4 \left(\frac{m}{10^{-14} \text{ eV}} \right)^3 \left(\frac{0.4 \text{ GeV/cm}^3}{\rho_{\text{IDM}}} \right) \left(\frac{v_{\text{IDM}}}{10^{-3}} \right), \quad (2.23)$$

where $\rho_{\text{IDM}} \simeq 0.4 \text{ GeV/cm}^3$ and $v_{\text{IDM}} \simeq 10^{-3}$ are the energy density and velocity dispersion, respectively, of local DM in the solar neighborhood vicinity (see e.g. [157] for review). Thus, on astrophysical timescales for sufficiently-strong self interactions, solar halos can collapse and explode multiple times for a given star, potentially converting a significant fraction of axionic DM to relativistic DaB constituents in the process.

- **Dark non-bosonic stars:** Astrophysical objects formed from SM particles (e.g. stars and NS) could have analogues in the dark sector, sometimes called *dark stars* [158, 159], composed of fermions rather than bosons. If their constituents are coupled to axions, they will be emitted by dynamical processes over a broad range of energies dictated by the dark star core temperature T_{dark} , which can be drastically distinct from $\sim \text{MeV}$ energies associated with ordinary astrophysical stars. An intriguing possibility is *mirror star*, formed from dark baryons in the context of complex dark sector models [160–162]. The constituents of dark stars and the interacting SM particles could contribute to axion emission, and therefore to the DaB. Population statistics and dynamics of such objects could be dramatically distinct from that of conventional astrophysical stars.
- **Secondary astrophysical axion production:** Secondary axions could be produced from decays of dark sector fields originating from various astrophysical processes, such as $\chi \rightarrow aa$ for a dark scalar χ . We note that this is distinct from cosmological DM decaying to axions (e.g. [67]).

Many relativistic axion emission mechanisms remain poorly understood without a well studied axion emission flux. Our analysis highlights the necessity and serves as an impetus for further detailed numerical studies and simulations required to comprehensively describe and quantify the axion emission mechanisms from distinct sources. A population of astrophysical sources that produces energetic axions can contribute to DaB.

2.3 Comparison to local DM flux

A simple estimate of DaB flux can be obtained as follows. Assuming a total density ρ_{loss} is converted into relativistic axions of average energy $\bar{\omega}$, ignoring redshift effects, the differential flux can be approximated as

$$\frac{d\phi}{d\omega} \sim \frac{\rho_{\text{loss}}}{\bar{\omega}^2} v_{\text{burst}}. \quad (2.24)$$

¹¹See also Ref. [150–156] for discussion of relaxation of ultralight fields through gravity and self-interactions.

This scaling can be roughly obtained from Eq. (2.15) in the approximation $dE/dk \rightarrow E_{\text{tot}}/\bar{\omega}$, $\sqrt{\omega^2 - m^2} \simeq \bar{\omega}$ and simultaneously setting $v_{\text{burst}} \rightarrow 1$, and ignoring the remaining prefactor. Similarly we can obtain this scaling from Eq. (2.12) in the limit¹² $\delta\omega \rightarrow 0$, $\omega \rightarrow \bar{\omega}$.

Using Eq. (2.24), we can estimate a typical ratio of axion background flux to that expected of cold axion DM. Given a local DM density of $\rho_{\text{IDM}} \simeq 0.4 \text{ GeV/cm}^3$ and velocity dispersion $v_{\text{IDM}} \simeq 10^{-3}$ (see e.g. [157] for review), the local DM flux is

$$\left(\frac{d\phi}{d\omega}\right)_{\text{IDM}} \sim \frac{\rho_{\text{IDM}}}{m^2} v_{\text{IDM}} \simeq 10^{26} \text{ eV}^{-1} \text{ cm}^{-2} \text{ sec}^{-1} \left(\frac{v_{\text{IDM}}}{10^{-3}}\right) \left(\frac{10^{-10} \text{ eV}}{m}\right)^2. \quad (2.25)$$

Comparing Eqs. (2.24-2.25), the expected ratio of DaB flux to DM flux to be

$$\frac{d\phi/d\omega}{(d\phi/d\omega)_{\text{IDM}}} \sim \left(\frac{v_{\text{burst}}}{v_{\text{IDM}}}\right) \left(\frac{m}{\bar{\omega}}\right)^2 \left(\frac{\rho_{\text{loss}}}{\rho_{\text{loc}}}\right) \simeq 3 \cdot 10^{-3} \mathcal{F} \left(\frac{m}{\bar{\omega}}\right)^2. \quad (2.26)$$

Compared to the local cold DM flux, the DaB flux is boosted by its relativistic velocity, $v_{\text{burst}}/v_{\text{IDM}} \sim 10^3$. However, it is suppressed by the small average DM density of the Universe relative to the expected local DM density, and by $\mathcal{F} < 1$, as $\rho_{\text{loss}}/\rho_{\text{loc}} \sim 10^{-6}\mathcal{F}$. Finally, for a fixed total energy output the DaB is suppressed by the larger energy per particle, ω , as $(m/\bar{\omega})^2 \ll 1$. Overall, the DaB flux is expected to be at least a few orders of magnitude below that of local cold axion DM in the solar neighborhood. We stress that these naive estimates do not account for redshift dependencies. Since the energy densities are larger at earlier times, converting a fixed axion DM fraction \mathcal{F} one could convert more axion DM by populations of transient sources at higher redshifts. Hence, Eq. (2.26) should be modified by $(1 + \bar{z})^3$ scaling when the source distribution is sharply peaked at some redshift \bar{z} in order to properly capture such behavior.

We illustrate the relativistic axion flux considering reference parameters (see Sec. 2.2), normalized to the local cold axion DM expectation as in Eq. (2.25), in Fig. 4. Here, for our estimates we assume a DM fraction $\mathcal{F} = 0.1$, and a Gaussian emission spectrum with a central energy $\bar{\omega} = 3m$ and with a width $\delta\omega = m$ (dashed) or $\delta\omega = m/10$ (thick). The left panel displays the results for a power-law distribution of sources with an exponent $p = 1$ (red) or $p = -1$ (purple), and $z_{\text{max}} = 5, 20$. For comparison, we also show the result for a Gaussian distribution with $\delta z = 0.1$ (red) or $\delta z = 3$ (purple), and $\bar{z} = 1, 10$ as labeled. We note that the DaB flux is within a few orders of magnitude of the flux expected from the local axion DM density, matching at the order-of-magnitude level to the rough estimates of Eq. (2.26), with a spread in energy that depends on the $\delta\omega$ as well as the cosmological history encoded in $R_{\text{burst}}(z)$.

Fig. 4 illustrates how the parameters of the cosmological rate function and burst spectrum determine the present-day flux in the DaB. For example, in the left panel (power-law rate function), extending the duration of the burst to higher redshifts, from $z_{\text{max}} = 5$ (faint lines)

¹²Here we use the identity $\sqrt{2\pi}\delta(x) = \lim_{\epsilon \rightarrow 0^+} \exp(-x^2/2\epsilon^2)/\epsilon$.

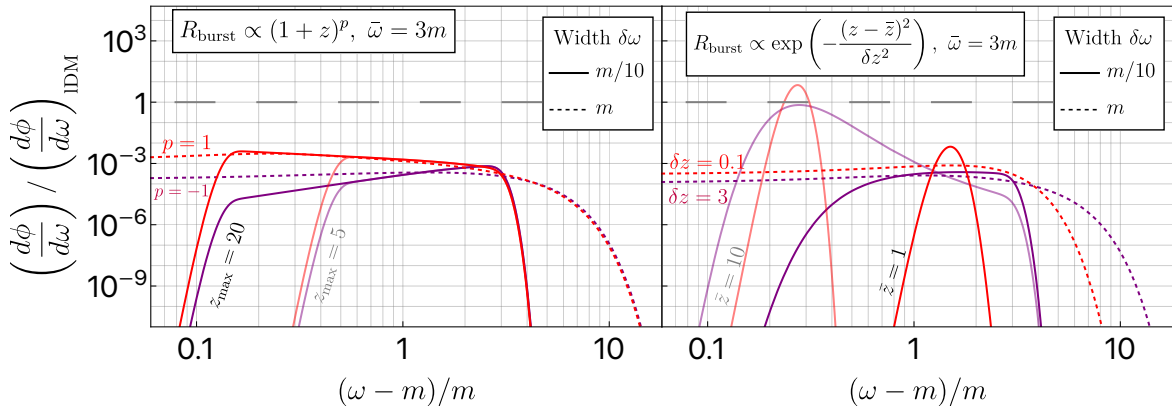


Figure 4: The differential flux, $d\phi/d\omega$, of DaB relative to the flux of cold axion DM in the local neighborhood, $(d\phi/d\omega)_{\text{IDM}}$, as a function of ω/m . For the source of the axion background, the thick (dashed) lines correspond to a Gaussian energy distribution at the source with peak energy $\bar{\omega} = 3m$ and width $\delta\omega = m$ ($m/10$). The cosmological rate function R_{burst} is given by: (Left panel) a power law $\propto (1+z)^p$ with $p = -1, 1$ and $z_{\text{max}} = 5, 20$ as illustrated; (Right panel) a Gaussian $\propto \exp[-(z - \bar{z})^2/\delta z^2]$ with $\bar{z} = 1, 10$ and $\delta z = 0.1, 3$ as illustrated.

to $z_{\text{max}} = 20$ (opaque lines) leads to a more significant low-energy component. The power-law exponent p , in contrast, has a more subtle effect on the present-day spectrum. For a Gaussian rate function, the peak energy after redshifting is found near $\bar{\omega}/(1 + \bar{z})$, and when the Gaussian width in redshift is smaller more of the energy remains near the peak, as in the red lines ($\delta z = 0.1$) compared to the purple ones ($\delta z = 3$). As we have demonstrated, at high redshift the DM density is higher than today, allowing a DaB flux larger than the DM background for example in case of Gaussian distribution at high redshift (shown by faint lines in the right panel of Fig. 4). In both panels, the dashed lines, which correspond to a larger width in energy $\delta\omega$, spread significantly in energy away from the initial peak at $\bar{\omega} = 3m$ than the solid lines, which exhibit a sharper cutoff.

Our analysis indicates that DaB flux could be sub-leading, and in some scenarios even dominate, compared to that of local cold axion DM. Successful detection of DaB flux would prove particularly valuable, providing unique information regarding the evolution of the axion field as well as its SM interactions in cosmological and astrophysical contexts dramatically distinct from cold DM. We further comment on direct-detection possibilities for DaB in Sec. 6.2.

3 Axion conversion to photons

Complementary to direct detection, the DaB can be probed through indirect signatures due to axion interactions with SM constituents. Prominent signals appear from axion conversion through axion-photon interaction of Eq. (2.2), either in the presence of magnetic

fields or through axion decays. We calculate the rates of axion-photon conversion for each scenario. The resulting photon signals can be searched for in a wide range of telescope and satellite experiments outlined in Sec. 4. Additional detectable DaB signatures could arise from other axion couplings as well, as we briefly discuss in Sec. 6.

3.1 Magnetic fields

Propagating axions, including those contributing to DaB from various sources as discussed in the previous section, can be efficiently converted (oscillate) to photons $a \rightarrow \gamma$ by astrophysical magnetic fields [163]. We shall subsequently focus on Milky Way Galactic magnetic fields. Consider axions traveling a distance R in a homogeneous magnetic field with a transverse component in the plane normal to direction of propagation B_T , which is of order μG in the Milky Way [164]. We assume Milky Way's magnetic field to be $B_T = 1 \mu\text{G}$ throughout. Then, the probability of conversion is [165]

$$P_{\gamma \rightarrow a} = (\Delta_{a\gamma} R)^2 \frac{\sin^2(\Delta_{\text{osc}} R/2)}{(\Delta_{\text{osc}} R/2)^2}, \quad (3.1)$$

where the oscillation wavenumber is $\Delta_{\text{osc}} \equiv \sqrt{(\Delta_a - \Delta_{\text{pl}})^2 + 4\Delta_{a\gamma}^2}$. We have considered the ultra-relativistic approximation, $\omega \gg m$, which we expect to be a generally reasonable approximation¹³. There are three distinct contributions to the conversion probability:

$$\Delta_{a\gamma} \equiv \frac{g_{a\gamma} B_T}{2} \simeq 1.5 \cdot 10^{-4} \left(\frac{g_{a\gamma}}{10^{-12} \text{ GeV}^{-1}} \right) \left(\frac{B_T}{\mu\text{G}} \right) \text{ kpc}^{-1}, \quad (3.2)$$

$$\Delta_a \equiv -\frac{m^2}{2\omega} \simeq -7.8 \cdot 10^{13} \left(\frac{m}{10^{-11} \text{ eV}} \right)^2 \left(\frac{10^{-10} \text{ eV}}{\omega} \right) \text{ kpc}^{-1}, \quad (3.3)$$

$$\Delta_{\text{pl}} \equiv -\frac{\omega_{\text{pl}}^2}{2\omega} \simeq -1.1 \cdot 10^{13} \left(\frac{n_e}{10^{-2} \text{ cm}^{-3}} \right) \left(\frac{10^{-10} \text{ eV}}{\omega} \right) \text{ kpc}^{-1}, \quad (3.4)$$

where $\omega_{\text{pl}} = \sqrt{4\pi\alpha n_e/m_e} \simeq 4 \cdot 10^{-11} \text{ eV} \sqrt{n_e/\text{cm}^{-3}}$ is the plasma frequency corresponding to effective mass that photons acquire induced by the SM background, with m_e being the electron mass and n_e density of free electrons in medium.

For lower energy emitted axions, when the energy scales could be semi-relativistic with ω are not very far from m , we find $\Delta_{a\gamma}$ is negligible at all relevant m . The other two contributing terms are equal, $\Delta_a \simeq \Delta_{\text{pl}}$, when $m = \omega_{\text{pl}}$. As indicated by Eqs. (3.3-3.4), both $|\Delta_a|, |\Delta_{\text{pl}}| \gg \text{kpc}^{-1}$ in this case. Hence, averaging the resulting fast oscillations in Eq. (3.1)

¹³In other energy regimes, we expect additional corrections.

as $\sin^2 \rightarrow 1/2$, we can write

$$\begin{aligned}
P_{\gamma \rightarrow a} &\simeq (\Delta_{a\gamma} R)^2 \frac{\sin^2(|\Delta_a - \Delta_{\text{pl}}| R/2)}{(\Delta_a - \Delta_{\text{pl}})^2 R^2/4} \\
&\simeq \begin{cases} 2 \left(\frac{\Delta_{a\gamma}}{\Delta_{\text{pl}}} \right)^2 \\ 2 \left(\frac{\Delta_{a\gamma}}{\Delta_a} \right)^2 \end{cases} \tag{3.5} \\
&= \begin{cases} 2 \cdot 10^{-32} \left(\frac{g_{a\gamma}}{10^{-12} \text{ GeV}^{-1}} \right)^2 \left(\frac{\omega}{10^{-10} \text{ eV}} \right)^2 \left(\frac{10^{-2} \text{ cm}^{-3}}{n_e} \right)^2 \left(\frac{B_T}{\mu\text{G}} \right)^2, & m \lesssim \omega_{\text{pl}}, \\ 4 \cdot 10^{-34} \left(\frac{g_{a\gamma}}{10^{-12} \text{ GeV}^{-1}} \right)^2 \left(\frac{\omega}{10^{-10} \text{ eV}} \right)^2 \left(\frac{10^{-11} \text{ eV}}{m} \right)^4 \left(\frac{B_T}{\mu\text{G}} \right)^2, & m \gtrsim \omega_{\text{pl}}. \end{cases}
\end{aligned}$$

Note that the result is essentially independent of R , since the argument of the sine function in Eq. (3.1) is significantly larger than unity for all astrophysical, and certainly cosmological, distances. In Fig. 5, we illustrate the two limits of Eq. (3.5) (red and blue curves, respectively), and compare to the full expression of Eq. (3.1) (purple). As indicated, the conversion probability is proportional to $P_{\gamma \rightarrow a} \propto g_{a\gamma}^2 \omega^2$.

In the other limiting regime, when $m \ll 10^{-11}$ eV and $\omega \gg \text{MeV}$ (as in e.g. environment of supernovae), the first term dominates and $P_{\gamma \rightarrow a}$ becomes independent of m and ω [54, 163]. In that case

$$P_{\gamma \rightarrow a} \simeq (\Delta_{a\gamma} R)^2 \simeq 2 \cdot 10^{-6} \left(\frac{g_{a\gamma}}{10^{-12} \text{ GeV}^{-1}} \right)^2 \left(\frac{B_T}{\mu\text{G}} \right)^2 \left(\frac{R}{\text{kpc}} \right)^2, \tag{3.6}$$

which approaches unity $P_{\gamma \rightarrow a} \rightarrow 1$ for sizable distances R . In panel (c) of Fig. 5 we illustrate the conversion probability for $R = \text{kpc}$ and for different axion energies $\omega = \text{keV}$, MeV , and GeV (purple, brown, and green lines respectively).

Using the above, in Sec. 4 below we estimate the sensitivity of experiments to detect photon signals generated by axion-photon conversion. For this, the flux of photons can be readily computed from DaB flux as

$$\left. \frac{d\phi_\gamma}{d\omega} \right|_{B\text{-field}} = P_{\gamma \rightarrow a} \frac{d\phi}{d\omega} \tag{3.7}$$

where the axion flux $d\phi/d\omega$ is given by Eq. (2.12). In what follows, we consider characteristic $R = 1 \text{ kpc}$, as the typical coherence length for Galactic magnetic fields is $\mathcal{O}(\text{few}) \text{ kpc}$ [164].

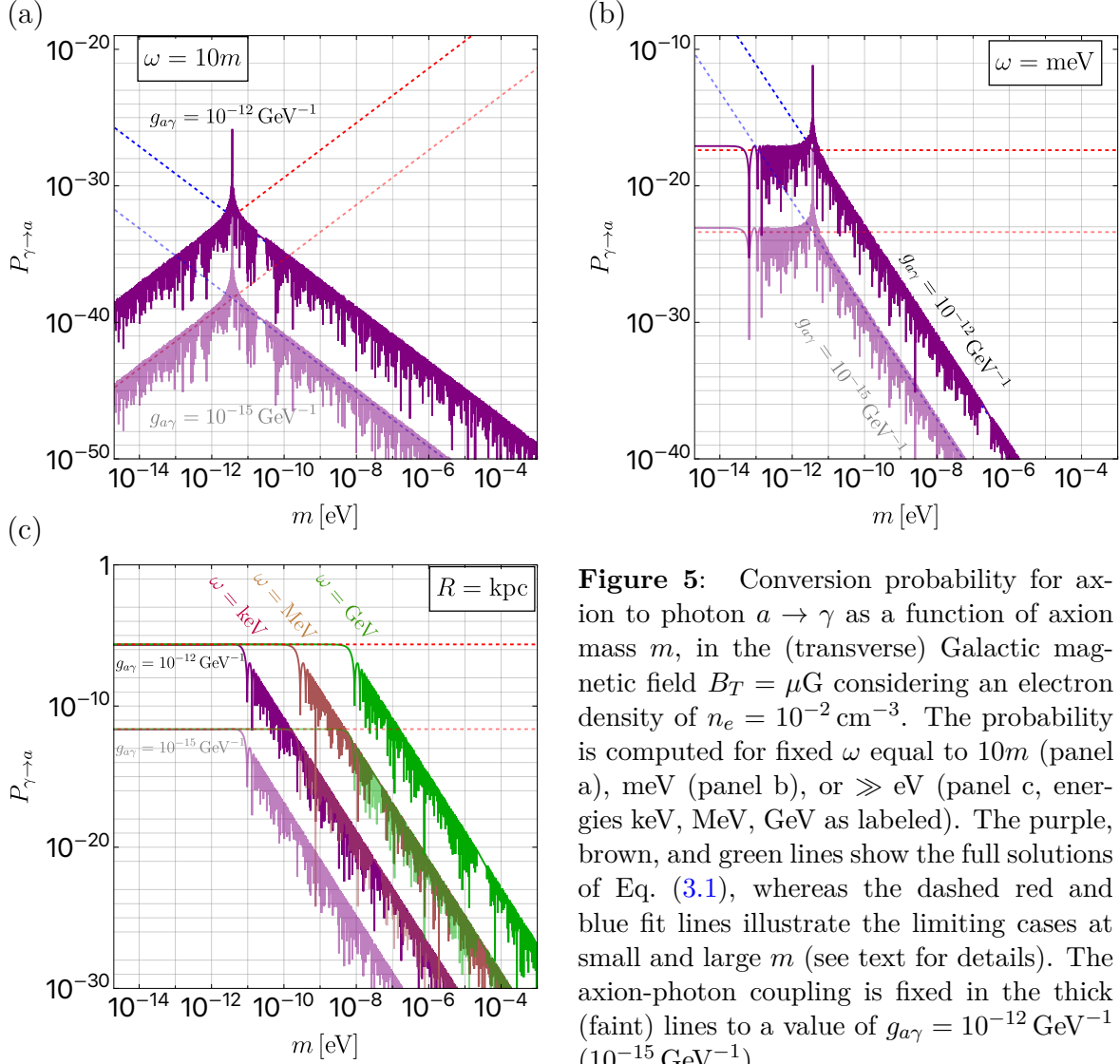


Figure 5: Conversion probability for axion to photon $a \rightarrow \gamma$ as a function of axion mass m , in the (transverse) Galactic magnetic field $B_T = \mu\text{G}$ considering an electron density of $n_e = 10^{-2} \text{ cm}^{-3}$. The probability is computed for fixed ω equal to $10m$ (panel a), meV (panel b), or $\gg \text{eV}$ (panel c, energies keV , MeV , GeV as labeled). The purple, brown, and green lines show the full solutions of Eq. (3.1), whereas the dashed red and blue fit lines illustrate the limiting cases at small and large m (see text for details). The axion-photon coupling is fixed in the thick (faint) lines to a value of $g_{a\gamma} = 10^{-12} \text{ GeV}^{-1}$ ($10^{-15} \text{ GeV}^{-1}$).

3.2 Axion decay

Axions can decay to photons, $a \rightarrow \gamma\gamma$, through the axion-photon coupling in Eq. (2.2). The decay rate of an axion in vacuum is given by

$$\Gamma_{\gamma\gamma} = \frac{g_{a\gamma}^2 m^3}{64\pi}. \quad (3.8)$$

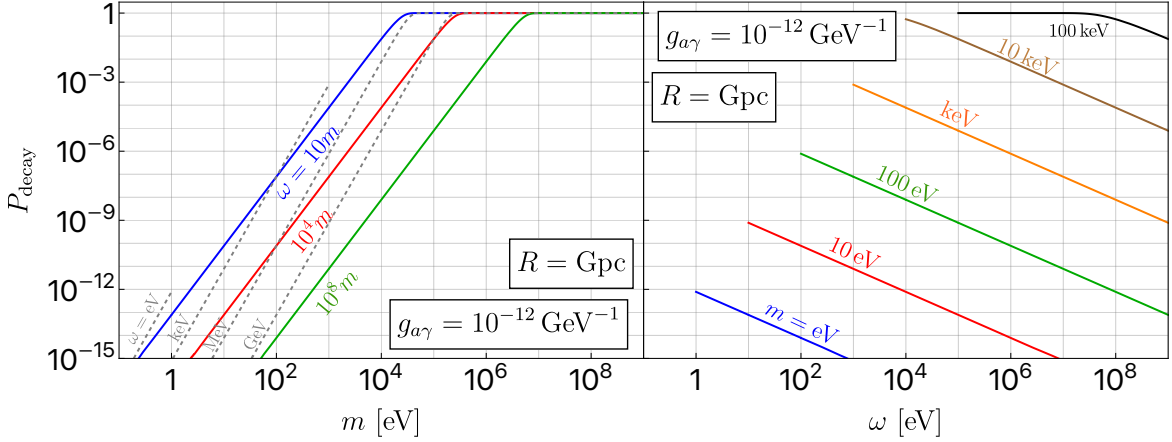


Figure 6: Axion-photon decay probability factor, P_{decay} , as a function of axion mass m at fixed energy ω (left panel), and as a function of axion energy ω at fixed mass m (right panel). Representative values of axion coupling $g_{a\gamma} = 10^{-12} \text{ GeV}^{-1}$ and cosmological propagation distance $R = \text{Gpc}$ are considered.

Hence, axions of energy ω traveling a distance R will decay with probability $P_{\text{decay}}(R, \omega) = 1 - \exp(-R/\ell(\omega))$, where the mean free path is given by

$$\ell(\omega) \simeq \frac{\gamma v_{\text{burst}}}{\Gamma_{\gamma\gamma}} \simeq \left(\frac{\omega}{m}\right) \frac{64\pi}{g_{a\gamma}^2 m^3} \simeq \text{Mpc} \left(\frac{\omega}{\text{MeV}}\right) \left(\frac{100 \text{ keV}}{m}\right)^4 \left(\frac{10^{-12} \text{ GeV}^{-1}}{g_{a\gamma}}\right)^2, \quad (3.9)$$

with γ is the relativistic Lorentz factor. As Eq. (3.9) illustrates, axions in the DaB can travel cosmological distances before decaying, and therefore the photon flux from decay must be computed self-consistently over cosmological redshifts z as

$$\left.\frac{d\phi_\gamma}{d\omega}\right|_{\text{decay}} = \int_0^\infty dz (1+z) \frac{dN_a(\omega(1+z))}{d\omega} R_{\text{burst}}(z) \left|\frac{dt}{dz}\right| 2P_{\text{decay}}(R(z), \omega(1+z)), \quad (3.10)$$

which accounts for the dependence of the source distance R and emission energy ω on redshift z . For a sharply-peaked distribution around some redshift \bar{z} , we can treat P_{decay} as a constant in the integration, and the decay flux takes the form

$$\left.\frac{d\phi_\gamma}{d\omega}\right|_{\text{decay}} \simeq 2P_{\text{decay}}(R(\bar{z}), \omega(1+\bar{z})) \frac{d\phi}{d\omega}, \quad (3.11)$$

which is analogous to Eq. (3.7) for magnetic field conversion. Note that there is an additional factor of 2 compared to magnetic field conversion case, since each axion decay creates two photons.

For example for Galactic contributions to DaB, such as from astrophysical supernovae, the distances to the sources R could be related to their astrophysical population distributions, e.g. localized around Galactic Center. More generally, particularly for dark sector sources,

the source distances $R(z)$ can be cosmological in scales, e.g. for $z \gtrsim 1$ we have $R(z) \gtrsim \text{Gpc}$, but depend in detail on the population distribution of axion emission sources. We define an effective redshift for the purpose of estimating the typical source distance in generality, z_{eff} , as

$$z_{\text{eff}} \equiv \frac{\int dt \frac{z R_{\text{burst}}(z)}{(1+z)^3}}{\int dt \frac{R_{\text{burst}}(z)}{(1+z)^3}}. \quad (3.12)$$

For a peaked distribution $R_{\text{burst}}(z)$, such as the Gaussian introduced in Eq. (2.7), Eq. (3.12) gives $z_{\text{eff}} \simeq \bar{z}$ to a good approximation if $\bar{z} \gtrsim 5$. For the power-law distribution in Eq. (2.7), which can be broader in redshift, z_{eff} is somewhat smaller, and we can approximate $z_{\text{eff}} \simeq 2/(7-2p)$. To estimate the decay probability in what follows, we use $R(z) \simeq 1/H(z_{\text{eff}})$ where $H(z)$ is the Hubble parameter.

As noted by Ref. [54], for large axion masses and energies $\omega, m \gtrsim \text{MeV}$ (appropriate for e.g. heavy axions produced in supernovae), nearly all axions are expected to decay on cosmological distances, as the exponential in Eq. (3.11) approaches zero, or equivalently when $R/\ell \gg 1$. On the other hand, when $R/\ell \ll 1$, we can approximate the flux as $d\phi_\gamma/d\omega \simeq (2R/\ell)d\phi/d\omega$, which is proportional to $\omega^{-1}m^4$ multiplied by the axion flux. We illustrate the behavior of P_{decay} in different limits in Fig. 6.

4 Observable signatures with photons

The generation of photon flux from DaB, either through magnetic B -field conversion or axion decays, allows to search for axions over a broad parameter space with a range of detectors and telescopes. In principle, the contributions from these processes are additive, stemming from the same axion-SM interaction $g_{a\gamma}$. However, as we demonstrated, the two processes are expected to contribute a significant flux of photons in distinct kinematic regimes. Approximately, axion magnetic field conversion tends to dominate at high energies when $\omega \gg m$ whereas axion decays are more prominent when their energy ω is within a few orders of magnitude of the mass m .

In Fig. 7 and Fig. 8, we illustrate the photon flux obtained from Galactic magnetic B -field conversion as well as axion decays, respectively. For comparison, we include the measured background flux from telescope experiments across a wide range of frequencies, from gamma-ray to radio, spanning nearly 20 orders of magnitude in photon energy. We observe that over a very broad parameter space, the photon flux obtained from DaB can greatly exceed other contributing backgrounds, allowing to impose constraints and promising future detection prospects.

Highlighting our results, we estimate in detail the sensitivity of several distinct experiments below. For concreteness, we consider a power-law distribution of cosmological transient sources $R_{\text{burst}} \propto (1+z)^p$ taking $p = -1$ and assuming a maximum redshift of $z_{\text{max}} = 20$. Computations of results for the case of power-law distribution of cosmological transient sources

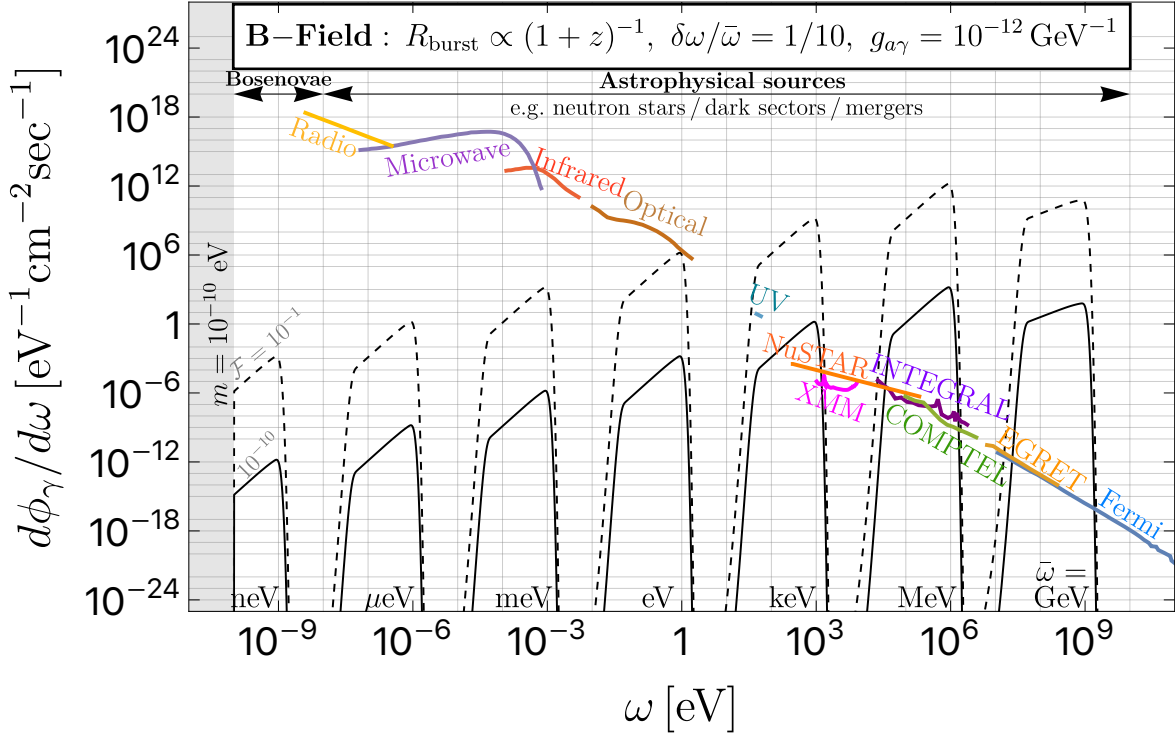


Figure 7: Photon flux from Galactic magnetic μG B -field conversion of the DaB (black lines) assuming $\mathcal{F} = 0.1$ (dashed) or 10^{-10} (thick), for axions with mass $m = 10^{-10} \text{ eV}$ and coupling $g_{a\gamma} = 10^{-12} \text{ GeV}^{-1}$ emitted from transient sources with cosmological burst rate $R_{\text{burst}} \propto (1+z)^{-1}$, ratio of central energy spread to average magnitude $\delta\omega/\bar{\omega} = 1/10$. Each pair of black lines corresponds to burst sources with central energy $\bar{\omega}$ as labeled along the x-axis. Contributing background fluxes for a wide range of photon frequencies (from radio, microwave, infrared, optical, and UV) are reproduced from Ref. [166] (see also references therein). At higher energies $\omega \gtrsim 100 \text{ eV}$, we display the photon flux measured by specific experiments, which lead to constraints on DaB, including NuSTAR [167, 168], XMM-Newton [169], INTEGRAL [170], COMPTEL [171, 172], EGRET [173], and Fermi-LAT [174, 175].

but with $p = 1$, as well as a Gaussian distribution, are depicted in App. A. We find the results for these cases to be overall similar to those presented below for power-law distribution with $p = -1$, suggesting that dependence on the detailed cosmological assumptions about transient source population is not very strong. Further, we find that the spread of the axion energy distribution, $\delta\omega/\bar{\omega}$, determines the position of the low-energy cutoff of each black curve.

4.1 Limits from X-ray and gamma-ray searches

Variety of experiments can sensitively probe flux of energetic photons with $\omega \gg \text{eV}$ from DaB. We illustrate this in Fig. 7 and Fig. 8, for selected input parameters, using the measured photon background flux of several existing experiments including NuSTAR [167, 168], XMM-

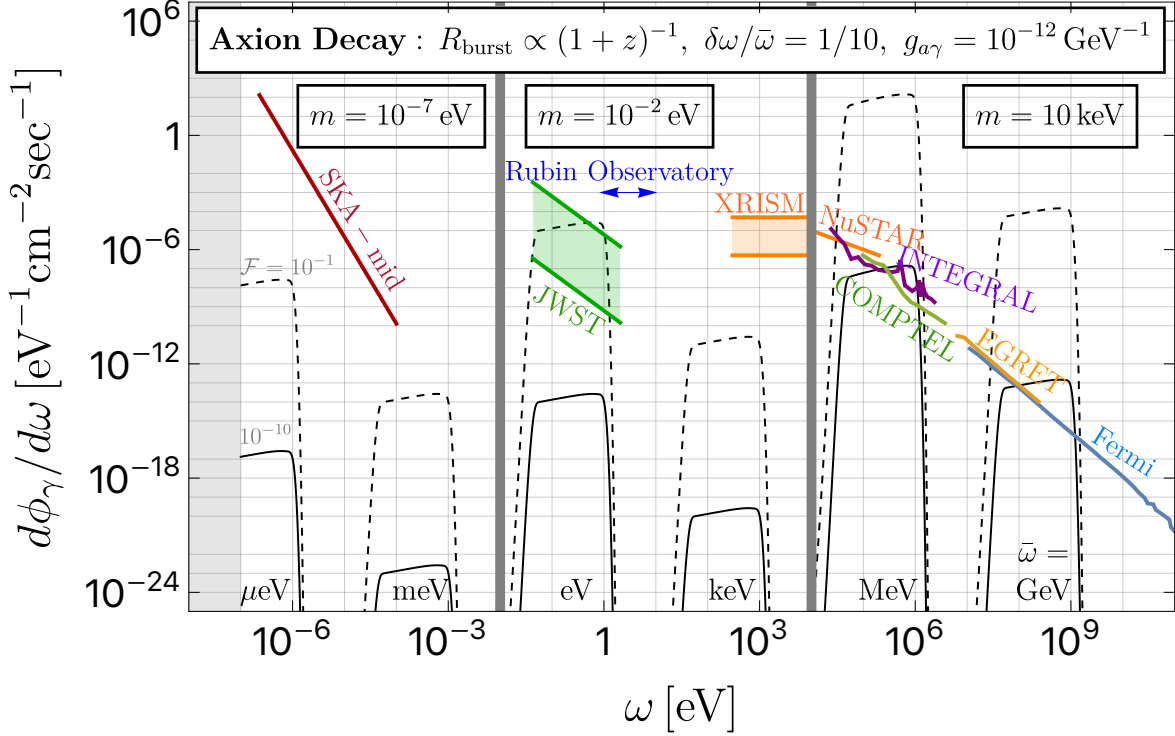


Figure 8: Photon flux from decay of axions from DaB (black lines) assuming $\mathcal{F} = 0.1$ (dashed) or 10^{-10} (thick), considering axion coupling $g_{a\gamma} = 10^{-12} \text{ GeV}^{-1}$ and mass $m = 10^{-7} \text{ eV}$ (left), 10^{-2} eV (center), and 10 keV (right). DaB is considered to arise from transient sources with cosmological burst rate of $R_{\text{burst}} \propto (1+z)^{-1}$, assuming typical source distance of $R(z_{\text{eff}}) \simeq 1/H(z_{\text{eff}})$ with $z_{\text{eff}} \simeq 2/9$. Each pair of black lines corresponds to transient sources with central energy $\bar{\omega}$ as labeled along the x-axis. (right) Photon fluxes measured by specific experiments and leading to constraints on DaB are as described in the caption of Fig. 7. At lower energies (below MeV, center, and below eV, left), we illustrate sensitivity of future searches by Vera C. Rubin Observatory (formerly LSST) [176, 177], JWST [178–181], XRISM [182] and SKA [183–185] as described in Sec. 4.2 (see also Fig. 10).

Newton [169], INTEGRAL [170], COMPTEL [171, 172], EGRET [173], and Fermi-LAT [174, 175]. As a characteristic example of Fermi-LAT, we consider 8-yr dataset observations of isotropic diffuse gamma-ray background¹⁴, which above can be modeled using a simple fit function [54]

$$\left. \frac{d\phi_\gamma(\omega)}{d\omega} \right|_{\text{Fermi}} \simeq 5.5 \cdot 10^{-10} \left(\frac{\text{GeV}}{\omega} \right)^{2.2} \text{ MeV}^{-1} \text{ cm}^{-2} \text{ sec}^{-1} \quad (4.1)$$

¹⁴ULTRACLEANVETO event class, with reduced cosmic-ray contamination. See iso_P8R3_ULTRACLEAN_V3_v1.txt at <https://fermi.gsfc.nasa.gov/ssc/data/access/lat/BackgroundModels.html>.

Experiment(s)	Energy Range	Flux ($d\phi_\gamma/d\omega$) Fit [$\text{eV}^{-1}\text{cm}^{-2}\text{sec}^{-1}$]
Radio* [166]	4 – 340 neV	$6.2 \cdot 10^{14} \left(\frac{\mu\text{eV}}{\omega}\right)^{1.5}$
Microwave* [166]	67 neV – 730 μeV	$3.2 \cdot 10^{17} \left(\frac{\omega}{\text{meV}}\right)^{0.5} \exp\left(-\frac{15\omega}{\text{meV}}\right)$
Infrared* [166]	0.1 – 5 meV	$6.3 \cdot 10^{13} \left(\frac{\omega}{\text{meV}}\right)^{0.5} \exp\left(-\frac{1.6\omega}{\text{meV}}\right)$
Optical* [166]	10 meV – 1.7 eV	$4.4 \cdot 10^6 \left(\frac{\text{eV}}{\omega}\right)^{1.8}$
UV* [166]	46 – 58 eV	$1.7 \cdot 10^4 \left(\frac{\text{eV}}{\omega}\right)^2$
NuSTAR [167, 168]	0.3 – 200 keV	$10^{-4} \left(\frac{\text{keV}}{\omega}\right)$
XMM-Newton [169]	1 – 8 keV	$8.9 \cdot 10^{-6} \left(\frac{\text{keV}}{\omega}\right)^{0.65}$
INTEGRAL [170]	24 keV – 2 MeV	$10^{-8} \left(\frac{\text{MeV}}{\omega}\right)^{1.6}$
COMPTEL [171, 172]	0.8 – 30 MeV	$5 \cdot 10^{-9} \left(\frac{\text{MeV}}{\omega}\right)^{2.4}$
EGRET [173]	6 – 240 MeV	$4 \cdot 10^{-16} \left(\frac{\text{GeV}}{\omega}\right)^{2.3}$
Fermi-LAT [174, 175]	30 MeV – 300 GeV	$5.5 \cdot 10^{-16} \left(\frac{\text{GeV}}{\omega}\right)^{2.2}$

* Denotes combined observations from multiple experiments [166].

Table 1: Summary of experiments whose observations are used to analyze photon signals from DaB derived in this work, along with their sensitivity energy range. The fits to the total measured photon flux in the Milky Way by experiments are also displayed. See Fig. 7 for further details.

in the ω energy range 30 MeV – 300 GeV. Analogously, COMPTEL observations [171] of diffuse gamma-ray emission can be fit as [54]

$$\left.\frac{d\phi_\gamma(\omega)}{d\omega}\right|_{\text{COMPTEL}} \simeq 5 \cdot 10^{-3} \left(\frac{\text{MeV}}{\omega}\right)^{2.4} \text{MeV}^{-1}\text{cm}^{-2}\text{sec}^{-1} \quad (4.2)$$

in the ω energy range 0.8 – 30 MeV. We summarize observations employed in our analysis in Tab. 1. Overall, we analyze combined observations in the ω energy range of approximately MeV – 300 GeV showcasing their implications for DaB, and leave a more comprehensive study of signals outside of this range to future work. Other measured fluxes, including those of EGRET, INTEGRAL, XMM, NuSTAR, and low-energy telescopes, are summarized in Tab. 1.

In order to obtain constraints on axion interactions, we vary the coupling $g_{a\gamma}$ to derive

the sensitivity regions for Fermi-LAT and COMPTEL, highlighting our analysis, where the peak photon fluxes from the DaB exceeds the gamma-ray fluxes displayed in Tab. 1. We stress that our analysis can be readily analogously carried out for other experimental observations (see e.g. Tab. 1). The resulting limits and constraints are illustrated in Fig. 9. The lines correspond to searches over the range of energies given in the legend, for COMPTEL (blue and red lines) and Fermi-LAT (green, yellow, and brown lines). As discussed previously, Galactic B -field conversion (see Eq. (3.7)) is most relevant for small axion masses $m \ll \text{eV}$, whereas decays (see Eq. (3.10)) dominate at larger axion masses. The change in the slope of the lines correspond to shifts in the behavior of the photon conversion and decay probabilities, seen in Fig. 5 and Fig. 6, respectively. For comparison, we also show the band corresponding to the QCD axion in pink [6–9].

The total flux is proportional to $\propto g_{a\gamma}^2 \mathcal{F}$, allowing for simple rescaling of our benchmarks for different DM fraction \mathcal{F} . We illustrate in Fig. 9 scenarios of $\mathcal{F} = 0.1$ and $\mathcal{F} = 10^{-20}$. We observe that even for a very small converted DM fraction $\mathcal{F} \lesssim 10^{-20}$, we find the estimated sensitivity for axions searches converting to photons due to Galactic magnetic fields far exceeds existing constraints from astrophysics or conventional direct DM detection searches using haloscopes (see Fig. 9 caption for details). At large masses, we find signals from axion decays can be competitive with strong existing cosmological limits [186].

We note that our estimates are conservative, since the photon flux associated with DaB could be detectable even if it is subdominant to background. Our analysis thus motivates dedicated searches, which would include detailed information about the distribution of DaB photons as a function of energy and could potentially significantly further improve these results.

4.2 Sensitivity of future searches

Rich opportunities exist to probe photons from DaB over a broad range of energies. Complementing observations at high energies $\omega \gg \text{eV}$ discussed in previous section, at low energies $\omega \lesssim \text{eV}$ there also exist significant backgrounds from radio, microwave, infrared, and optical frequency photons, as summarized in Fig. 7. However, many recently-launched as well as proposed future experiments are expected to probe significantly smaller fluxes over a wide range of energies. These include the Square Kilometer Array (SKA) with sensitivity in the radio range $\omega < 10^{-4} \text{eV}$ [183–185], Vera C. Rubin Observatory¹⁵ operating at optical energy range 1–10 eV [176, 177], James Webb Space Telescope (JWST) sensitivity in the infrared of 0.04–2 eV [178–181], recently launched XRISM with sensitivity for X-rays of 0.3–12 keV [182], as well as the e-ASTROGAM and AMEGO proposals with sensitivity for gamma rays in the range of 0.1 MeV – 300 MeV, estimated as having similar sensitivity [217–220].

We estimate, see App. B for details, the expected photon background flux observations from experiments and illustrate comparison with the DaB flux in Fig. 10. We note that

¹⁵Formerly, Large Synoptic Survey Telescope, LSST.

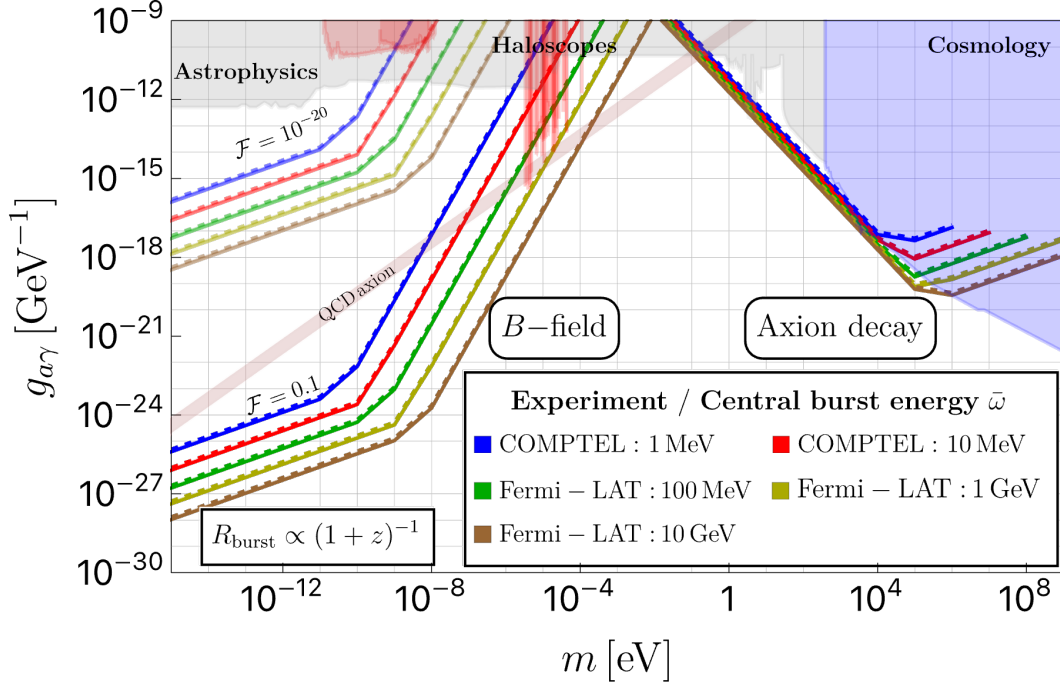


Figure 9: Sensitivity to DaB photons of COMPTEL (blue, red) and Fermi-LAT (green, yellow, and brown), as a function of axion mass m for average transient burst energy $\bar{\omega}$. The emitted photons are produced from either Galactic magnetic μG B -field conversion (left side) or axion decays (right). DaB is considered to arise from transient sources with cosmological burst rate of $R_{\text{burst}} \propto (1+z)^{-1}$. For B -field conversion we take $R = \text{kpc}$, and for axion decay we assume a typical source distance of $R(z_{\text{eff}}) \simeq 1/H(z_{\text{eff}})$ with $z_{\text{eff}} \simeq 2/9$. The upper (lower) lines correspond to $\mathcal{F} = 0.1$ ($\mathcal{F} = 10^{-20}$). The thick (dashed) lines correspond to transient burst with energy spread $\delta\omega = \bar{\omega}/10$ ($\delta\omega = \bar{\omega}$). For enumeration of astrophysical limits (gray) below $m \lesssim 0.1$ eV, see Fig. 12. At $m \gtrsim 0.1$ eV we also include astrophysical limits (gray) from the Hubble Space Telescope (HST) [187], James Webb Space Telescope (JWST) [180], the Visible Multi-Object Spectrograph (VIMOS) [188], MUSE-Faint survey [189], and the Breakthrough Listen Galactic Center Survey [190], as well as direct DM detection searches using haloscopes (red) including ADMX [191–196], CAPP [197–203], CAST-CAPP [204], CAST-RADES [205], GrAHal [206], RBF [207], HAYSTAC [208–210], QUAX [211–213], ORGAN [214, 215], and TASEH [216]. For $m \gtrsim 100$ eV we illustrate leading constraints from cosmology (blue) from Ref. [186].

precise sensitivity estimates could depend on a multitude of relevant factors, such as the source, telescope direction, noise estimates as well as duration.

To showcase different detection approaches, we highlight the sensitivity estimate of SKA to the flux of photons from DaB.¹⁶ SKA is expected to have unprecedented sensitivity reach at low radio energies $\omega < 10^{-4}$ eV and the methodology is qualitatively distinct from that of

¹⁶SKA analysis has also been performed to search for decay of cosmological DM to axions, $\chi \rightarrow aa$, which subsequently convert to photons [67].

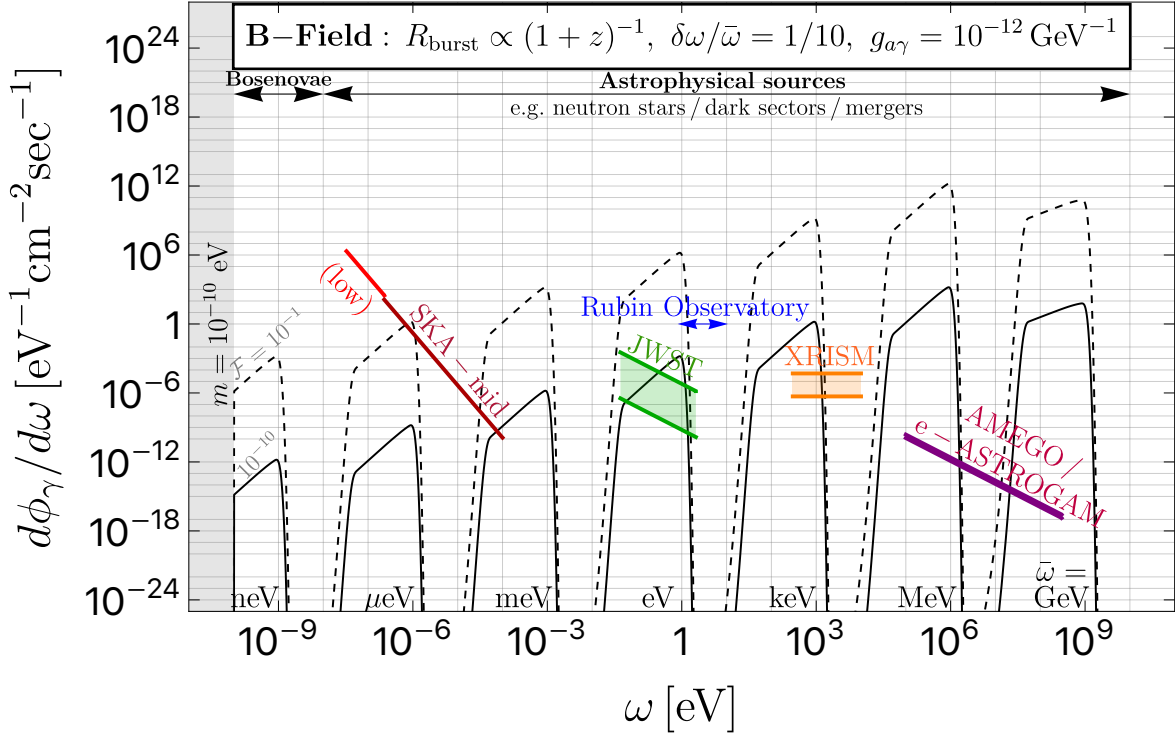


Figure 10: Same as Fig. 7, but illustrating the expected sensitivity of recently-launched and future experiments (see App. B and references for flux estimation) including SKA [183–185], Vera C. Rubin Observatory (formerly LSST) [176, 177], JWST [178–181], XRISM [182], and gamma-ray proposals e-ASTROGAM and AMEGO [217–220]. Note that the blue arrows labeled “Rubin Observatory” denote only a range of sensitivity in ω , not a photon flux sensitivity estimate.

searches with high-energy gamma-ray telescopes, such as Fermi-LAT as discussed in previous Sec. 4.1. Expected performance of SKA can be found in Ref. [184]. We consider two planned realizations of the experiment: *SKA-low*, with a collecting surface area of $A \simeq 419,000 \text{ m}^2$ and operating in the 50 – 350 MHz frequency range, and *SKA-mid*, with a collecting surface area of $A \simeq 10^6 \text{ m}^2$ (i.e. 5659 antennas with 15 m diameter) and detection range of 350 MHz – 15.4 GHz. For both configurations we assume a detection efficiency of $\eta \simeq 0.8$.

The experimental sensitivity can be conventionally estimated via by comparing the total power in the signal, P_{sig} , to the power in the noise, P_{noise} . The signal power can be calculated from the differential flux as

$$P_{\text{sig}} = \eta AS . \quad (4.3)$$

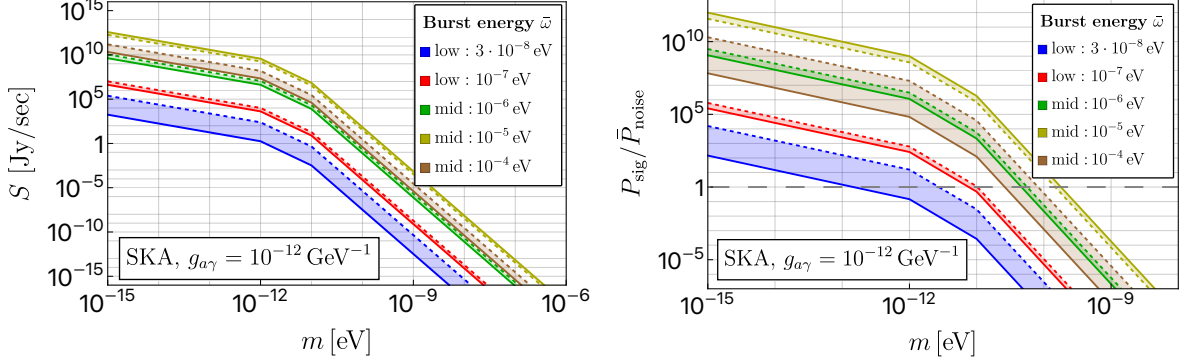


Figure 11: (Left) Total integrated photon flux density S , as described by Eq. (4.4). (Right) Detection signal-to-noise ratio $\text{SNR} = P_{\text{sig}}/\bar{P}_{\text{noise}}$ (right panel) in the sensitivity range of SKA-low (blue, red) as well as SKA-mid (green, yellow, brown), as a function of axion mass m for an average transient emission burst energy $\bar{\omega}$. The thick (dashed) lines correspond to burst emission energy spread of $\delta\omega = \bar{\omega}/10$ ($\delta\omega = \bar{\omega}$). DaB is considered to arise from transient sources with cosmological burst rate of $R_{\text{burst}} \propto (1+z)^{-1}$ and with $\mathcal{F} = 0.1$.

The integrated flux density, S , is defined by¹⁷

$$S \equiv \int_{\omega_1}^{\omega_2} d\omega \omega \frac{d\phi_\gamma}{d\omega}. \quad (4.4)$$

We estimate the flux density S in Fig. 11 for several choices of average transient burst energy $\bar{\omega}$.

The system’s noise can be described by Dicke’s radiometric receiver formula [221]

$$P_{\text{noise}} = T_{\text{sys}} \sqrt{\frac{\Delta\nu}{t_{\text{obs}}}}, \quad (4.5)$$

where $\Delta\nu$ is the frequency bandwidth in the experiment, t_{obs} is the observation time, T_{sys} is the system noise temperature. We consider the following contributions to the system noise temperature

$$T_{\text{sys}} = T_{\text{atm}} + T_{\text{CMB}} + T_{\text{bknd}} + T_r, \quad (4.6)$$

where $T_{\text{atm}} \simeq 3 \text{ K}$ [222] is the atmospheric sky emission temperature, $T_{\text{CMB}} = 2.725 \text{ K}$ is the cosmic microwave background (CMB) radiation temperature, T_{bknd} is the sky brightness temperature contributed by emission of all “background” radio sources and T_r is the noise contributed by radiometric receiver itself. For SKA-low (mid), we take an approximate averaged contribution over frequency bands of $T_r \simeq 20$ (40) K [184]. The background source

¹⁷Conventionally, this is measured in Janskys (Jy) per second. Recall that $1 \text{ Jy} = 10^{-23} \text{ erg cm}^{-2} \simeq 6.2 \cdot 10^{-12} \text{ eV cm}^{-2}$.

emission temperature can be estimated as [184, 185]

$$T_{\text{bknd}} \simeq 60 \text{ K} \left(\frac{300 \text{ MHz}}{\nu} \right)^{2.55}. \quad (4.7)$$

Converting the noise power P_{noise} in Eq. (4.5) to an equivalent flux, we arrive at the red lines in Fig. 7 and Fig. 8. As a simple noise model for our study, we use the noise averaged over the frequency range of each experiment

$$\bar{P}_{\text{noise}} \equiv \frac{1}{\Delta\nu} \int P_{\text{noise}}(\nu) d\nu. \quad (4.8)$$

For SKA-low (SKA-mid) we have $\bar{P}_{\text{noise}} \simeq 0.3$ (0.17) eV/sec.

Defining the signal-to-noise-ratio parameter $\text{SNR} \equiv P_{\text{sig}}/\bar{P}_{\text{noise}}$, we also illustrate the sensitivity region for SKA for the same benchmarks in $\bar{\omega}$ in the right panel of Fig. 11. As before, the slope of the lines changes when the behavior of the photon conversion probability changes, near $10^{-12} - 10^{-11}$ eV, as seen in Fig. 5(b). In order to determine sensitivity to axions contributing to DaB, as before we vary coupling $g_{a\gamma}$ values to find sensitivity regions where $\text{SNR} > 2$. The results are shown in Fig. 12. We observe that SKA can efficiently detect DaB signatures for sources with central burst energies $\bar{\omega} \simeq 10^{-8} - 10^{-4}$ eV over a wide range of axion masses $m \lesssim 10^{-9}$ eV. We note that the precise sensitivity depends on the assumed cosmological population distribution of transient burst sources, as further discussed in App. A.

5 Case study: axion star bosenovae

As demonstrated, photons arising from DaB constitute promising targets for future searches. Our analysis can hence be utilized to set constraints on and probe the existence of transient sources of relativistic axion emission as well as their population distributions originating from distinct theories of new physics.

As an example, we outline the analysis steps for the scenario of relativistic axions emitted from the bosenovae that are the endpoint evolution of collapsing boson stars [38, 39], discussed in Sec. 2.2.2. Importantly, the axion emission spectrum of the source in this case, $dN_a(\omega)/d\omega$, has been precisely determined by dedicated numerical simulations [39]. We can model the leading relativistic peak as shown in Fig. 3, which has central axion emission energy of $\bar{\omega} \simeq 2.2m$ and energy spread of $\delta\omega \simeq 0.4m$, using Gaussian distribution described in Eq. (2.10). On the other hand, the cosmological history and transient rate of bosenovae remains poorly understood and can depend on multiple complex processes. For illustration, we adopt a power-law cosmological bosenovae source distribution of Eq. (2.7) with parameter $p = -1$, and analyze the resulting constraint on \mathcal{F} assuming non-observation of signals in experiments.

With above approximations, one can compute the total flux in DaB using Eq. (2.12). Assuming boson stars are formed from ultralight particles, $m \ll \text{eV}$, and the energy scale of emission is of order $\bar{\omega} \sim 2.2m$, we will be interested in low-energy signals detectable by SKA. In this parameter range, axion decays rather than Galactic magnetic field axion conversion

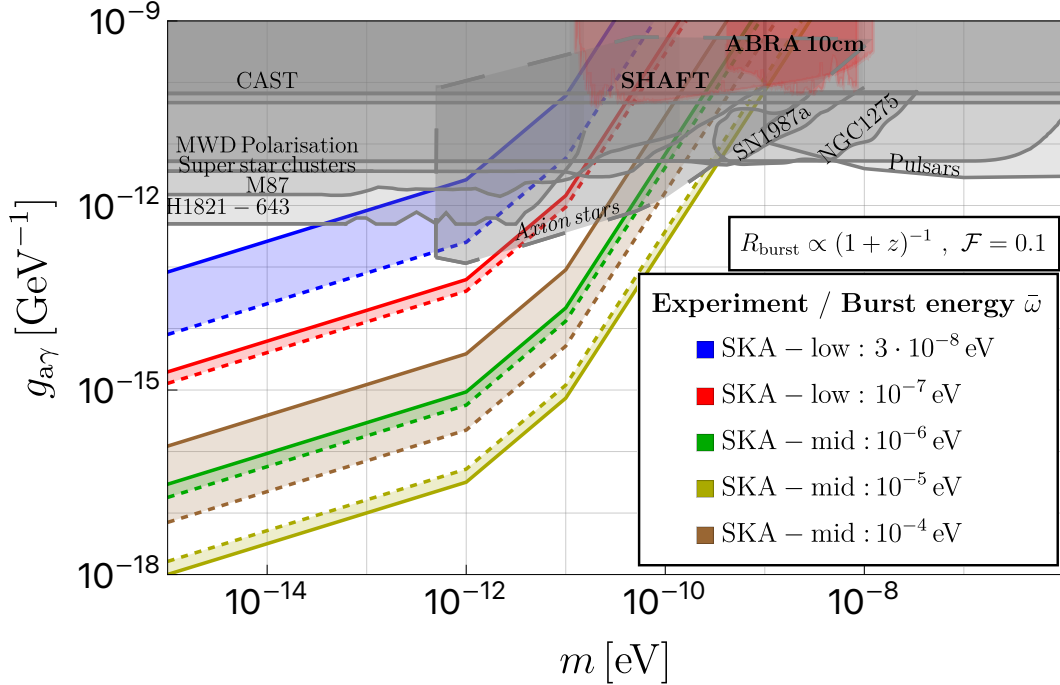


Figure 12: Sensitivity estimation for SKA-low (blue, red) and SKA-mid (green, yellow, and brown) to detect DaB, as a function of axion mass m for average transient burst energy $\bar{\omega}$. The dominant axion-photon conversion process in this region is through the Galactic magnetic B-fields (see Eq. (3.7)). The thick (dashed) lines correspond to transient burst energy spread of $\delta\omega = \bar{\omega}/10$ ($\delta\omega = \bar{\omega}$). DaB is considered to arise from transient sources with cosmological burst rate of $R_{\text{burst}} \propto (1+z)^{-1}$ and with $\mathcal{F} = 0.1$. Existing constraints are overlaid in gray including astrophysical limits (only leading limits shown, see e.g. Ref. [17, 223] for a more comprehensive list) from Chandra (H1821-643 [224], M87 [225], and NGC1275 [226] sources), super star clusters [227], magnetic white dwarf (MWD) polarization [228], CAST [229, 230], pulsar polar-cap cascades [143], and SN1987a [99, 231], direct detection limits (red) from SHAFT [232] and ABRA 10cm [233] as well as cosmology-dependent limit from axion star explosions inducing early-Universe heating of the intergalactic medium shown with gray long-dashed line [116, 117].

dominates the production of photons. Therefore, we employ Eq. (3.10) to determine the total flux of photons, and Eq. (4.3) as well as Eq. (4.4) to determine the total signal power.

We vary $g_{a\gamma}$ to determine the sensitivity region where $\text{SNR} \equiv P_{\text{sig}}/\bar{P}_{\text{noise}} > 2$. The results are shown in Fig. 13 for SKA-low (blue) as well as SKA-mid (green). For the benchmark we used above, $\mathcal{F} = 0.1$, the best projected sensitivity in the SKA range is $g_{a\gamma} \gtrsim 10^{-10} \text{ GeV}^{-1}$ at $m \simeq 10^{-5} \text{ eV}$, which is weaker than existing astrophysical constraints (shaded gray region). To reach the sensitivity in axion coupling of the order of $g_{a\gamma} \simeq 10^{-12} \text{ GeV}^{-1}$, DaB DM fraction would need to exceed $\mathcal{F} \simeq 10^3$, as can be readily seen from SNR scaling of $\propto \mathcal{F} g_{a\gamma}^2$. For illustration, in Fig. 13 we also display the sensitivity reach considering the unphysical bench-

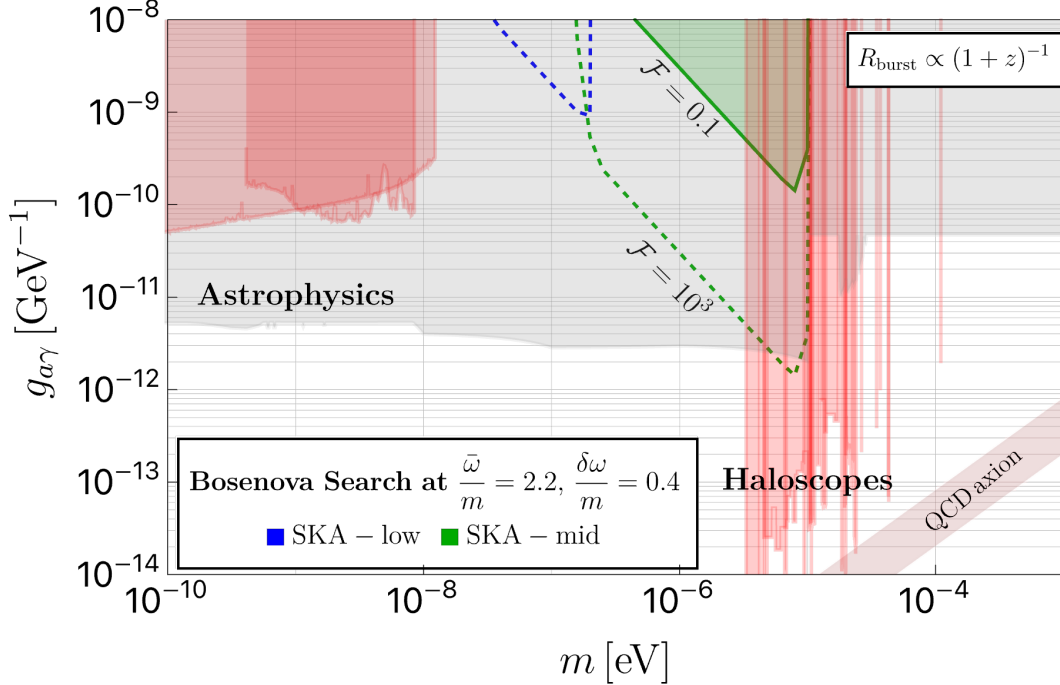


Figure 13: Sensitivity estimate for photons from the DaB associated with axion bosonovae, with emission spectrum modeled as Gaussian with average energy $\bar{\omega} = 2.2m$ and spread $\delta\omega = 0.4m$, considering SKA-low (blue lines) or SKA-mid (green). In this range, the flux is dominated by photons produced from axion decay (see Eq. (3.10)). The solid lines correspond to $\mathcal{F} = 0.1$, while the dashed lines have $\mathcal{F} = 10^3$. DaB is considered to arise from bosonovae with cosmological burst rate of $R_{\text{burst}} \propto (1+z)^{-1}$. Constraints from astrophysics and haloscopes are further described in the caption of Fig. 9.

mark of $\mathcal{F} = 10^3$. The results are similar for other cosmological bosonovae rate distribution functions, including Gaussian analyzed in App. A.

This example illustrates how DaB can be exploited to constrain the distribution of relativistic transient axion bursts from a source population with a known emission spectrum, in this case bosonovae. Such search also represents a complementary approach to existing ones that can probe couplings near the astrophysical limits. Based on the results above, we expect improved sensitivity for more energetic axion emission bursts, with $\bar{\omega} \gg m$ (see Sec. 4.2), or for astrophysical sources giving rise to X-ray or gamma-ray signals (see Fig. 7 and Fig. 8). Extrapolating this study to larger m , our results also motivate high-sensitivity next-generation experiments at frequencies above 15 GHz where SKA-mid loses sensitivity, which may lead to novel constraints on the DaB. We leave detailed investigation of such sources to future work.

6 Complementary search prospects

6.1 Axion-electron and other couplings

While we have focused on axion couplings to photons, other axion couplings (see Eq. (2.3)) could give rise to different novel signals associated with DaB and call for dedicated analyses.

As an example, consider the coupling to electrons of the form $\mathcal{L} \supset (g_{ae}/2m_e)(\partial_\mu a)\bar{e}\gamma^\mu\gamma_5 e$, where m_e and e are the electron mass and field, and g_{ae} is the dimensionless axion-electron coupling. If the axions have mass greater than twice the electron mass, $m \gtrsim 2m_e \simeq \text{MeV}$, this creates a new decay channel for the DaB and could be searched for in a wide range of experiments. Note that if the electron coupling is present at tree level, there is no analogue of magnetic-field conversion that we described for photon couplings. However, photon couplings could be induced beyond tree level, e.g. through a loop of electrons with tree-level coupling given by Eq. (2.3), implying a potentially interesting interplay between the two [54].

The typical decay length for the process $a \rightarrow \bar{e}e$ is given by [234, 235]

$$\ell_e = \frac{\gamma v_{\text{burst}}}{\Gamma_{e^+e^-}} = 8 \cdot 10^{-5} \text{ pc} \left(\frac{10^{-13}}{g_{ae}} \right)^2 \left(\frac{20 \text{ MeV}}{m} \right)^2 \left(\frac{\omega}{100 \text{ MeV}} \right) \left[\frac{1 - \left(\frac{m}{\omega} \right)^2}{1 - \left(\frac{2m_e}{m} \right)^2} \right]^{1/2}, \quad (6.1)$$

where we used¹⁸ $\Gamma_{e^+e^-} \simeq (g_{ae}^2/8\pi)\sqrt{m^2 - 4m_e^2}$. Compared with the case of axion decays to photons, c.f. Eq. (3.9), the decay length associated with axion electron decays tends to be significantly shorter, but is restricted to sizable $m \gtrsim 2m_e$. The flux of electrons and positrons from axion decays is similar to the photon case in Eq. (3.10), and is given by

$$\left. \frac{d\phi_e}{d\omega} \right|_{\text{decay}} = \int_0^\infty dz(1+z) \frac{dN_a(\omega(1+z))}{d\omega} R_{\text{burst}}(z) \left| \frac{dt}{dz} \right| 2P_{\text{decay}}^{(e)}(R(z), \omega(1+z)), \quad (6.2)$$

where $P_{\text{decay}}^{(e)}(R, \omega) = [1 - \exp(-R/\ell_e(\omega))]$ is the decay probability. The flux reduces, as in Eq. (3.11), to

$$\left. \frac{d\phi_e}{d\omega} \right|_{\text{decay}} \simeq 2P_{\text{decay}}^{(e)}(R(\bar{z}), \omega(1+\bar{z})) \frac{d\phi}{d\omega}, \quad (6.3)$$

when $P_{\text{decay}}^{(e)}$ is independent of redshift, e.g. for a rapid epoch of bursts at a fixed redshift $z = \bar{z}$. Here we sum the flux of electrons and positrons together.

For cosmological distances $R \sim \text{Gpc}$, the decay probability generally tends to unity $P_{\text{decay}}^{(e)} \rightarrow 1$ when the axion-electron coupling values are near the current experimental limits for light axions, $g_{ae} \simeq 10^{-13}$ (see e.g. [237]). Hence, one expects nearly all sufficiently heavy axions contributing to DaB to decay to electrons. For illustration, in Fig. 14 we demonstrate that even for a significantly smaller coupling $g_{ae} = 10^{-18}$ a significant fraction of the DaB is expected to decay, providing opportunities for related signatures.

¹⁸This also matches Ref. [236], taking $g_{ae} = c_{\ell\ell}^{\text{eff}} m_\ell/\Lambda$.

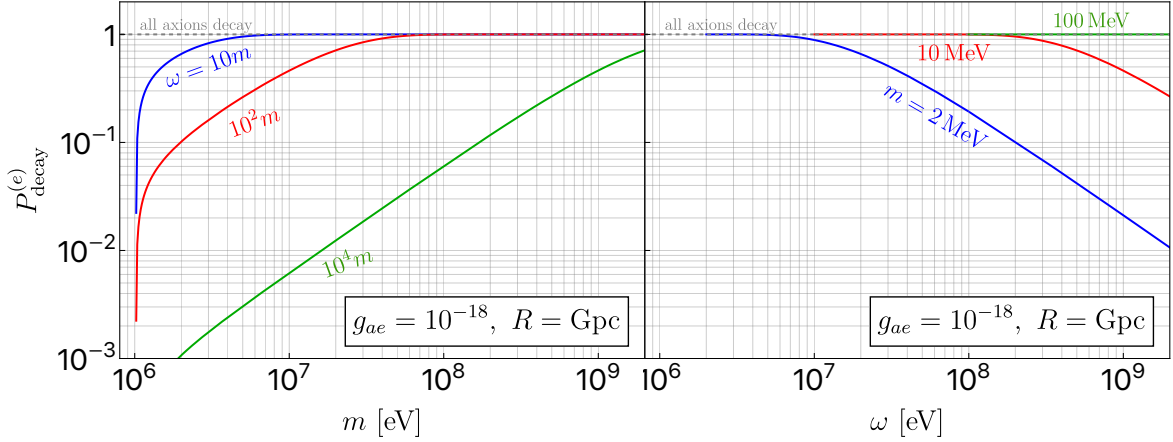


Figure 14: Axion-electron decay probability, $P_{\text{decay}}^{(e)}$, as a function of axion mass m and a fixed energy ω (left panel), and as a function of energy ω at fixed mass m (right panel). Reference values of coupling $g_{ae} = 10^{-18}$ and distance $R = \text{Gpc}$ are considered.

Electrons and positrons produced by the DaB can serve as novel efficient sources of photons. For astrophysical sources inside the Galaxy, primary mechanisms include interactions with interstellar medium gas, Galactic magnetic fields, or interstellar radiation fields including the cosmic microwave background (CMB). These can lead to production of X-ray and γ -ray photons, serving as targets for experiments like XMM-Newton, INTEGRAL and COMPTEL, as has been shown for positrons originating in decays of astrophysical supernova axions [238, 239]. Our analysis also highlights the significance of distinct sources producing axions contributing to DaB and their energetics. As we have demonstrated, for example, axion decay probability can be dramatically different between the ultrarelativistic source emission with $\omega \gg m$ and semi-relativistic source emission with $\omega \sim m$.

However, the DaB flux need not originate from within the Galaxy, particularly in case of dark sector sources, allowing for other search approaches as we outline. In analogy to the scenario of decaying DM (e.g. [240–242]), DaB contributions to extragalactic γ -ray background can arise from Inverse Compton scattering off the CMB. Unlike decaying DM case, the origin of decaying particles is not associated with a constant DM density but depends on the cosmological redshift distribution of axion emission sources as specified by R_{burst} model. We can thus estimate the flux of photons of energy ω in generality as

$$\begin{aligned} \left. \frac{d\phi_\gamma}{d\omega} \right|_{\text{decay}} &= \int_0^\infty dz (1+z) R_{\text{burst}}(z) \left| \frac{dt}{dz} \right| \\ &\times \int d\omega_e \int d\omega_{\text{CMB}} \int_{\omega_e}^\infty d\omega' P_{\text{decay}}^{(e)}(R(z), \omega'(1+z)) \frac{dN_a(\omega'(1+z))}{d\omega'} Q(\omega, \omega', \omega_e, \omega_{\text{CMB}}), \end{aligned} \quad (6.4)$$

where $Q(\omega, \omega', \omega_e, \omega_{\text{CMB}})$ is a function characterizing the photon production from electron and positron conversion originating from DaB associated with Inverse Compton scattering

against CMB photons. Here, the integrations are taken over the distribution of CMB energies ω_{CMB} , electron energies ω_e , and axion energies ω' . The flux of photons will also experience attenuation. We leave detailed computations of realizations of such scenarios and discussion of resulting constraints for future work.

Other potentially promising scenarios for observations can also arise from axions coupled to gluons or quarks, as is the case for QCD axions. In such case, axions can decay hadronically. For $m \lesssim 1$ GeV, the dominant decays are $a \rightarrow 3\pi^0$ and $a \rightarrow \pi^+\pi^-\pi^0$ [236], with neutral pions subsequently decaying primarily into photons $\pi^0 \rightarrow \gamma\gamma$ and charged pions into muons and neutrinos. We leave detailed discussion of these possibilities for future studies.

6.2 Direct detection

While we have focused on indirect DaB searches, direct searches are possible and complementary. Here, we briefly describe prospects and advantages of DaB direct detection.

As computed in Sec. 2.3, the total flux from DaB is generally sub-leading compared to the flux of local DM in the solar neighborhood vicinity. However, in some scenarios, we found that DaB flux can even be larger than the expected local DM flux. A direct search for DaB in terrestrial axion experiments could be viable for a number of reasons. First, the frequency range of interest is shifted from around axion mass m , associated with non-relativistic cold axion DM described by Maxwell-Boltzmann distribution with velocity dispersion of $v_0 \simeq 220$ km/s (e.g. [157] for review), to $\omega \gg m$ for relativistic axions, allowing for additional sensitivity to very light fields. Further, the broad distribution of axion energies contributing to DaB is also distinct from the narrow distribution expected of cold DM, see Fig. 4. It is also worth noting that the very local DM density, on scales of \sim AU-pc within our solar neighborhood, is not well-known [243, 244], and can deviate from the conventionally-assumed value of ρ_{loc} .

DaB direct detection searches are complementary to direct detection searches of relativistic axions from transient sources, as analyzed in Ref. [49, 51, 52]. Importantly, the presence of DaB constitutes continuous signals with expected constant density in experiments. On the other hand, transient signals result in temporary flux density increases of axions traversing the experiments, which depending on effects such as wave-spreading can be nearly instantaneous or lasting even months or years [49, 51]. While the DaB flux depends on the population distribution of axion emission sources, persistent associated signals do not require existence of a particular transient source emitting axions recently or near the Earth. We also note searches for DaB are complementary to *cosmological* sources of relativistic axions, the so-called cosmic axion background [18–20], which are limited by the number of relativistic degrees of freedom in the early Universe, N_{eff} , and also are diminished by significant redshifting of axion energies when $z \gtrsim 1000$.

For axions of mass $m \lesssim$ eV, the integration of coherent oscillations over long timescales poses a significant source of experimental sensitivity. For such oscillations this is characterized by a coherence timescale $\tau \simeq 2\pi(mv^2)^{-1}$ for axion velocity v , which corresponds to an oscillator quality factor $Q \equiv v^{-2}$. For cold DM in the solar neighborhood vicinity,

$Q_{\text{IDM}} \simeq v_{\text{IDM}}^{-2} \simeq 10^6$, and for transient bosenovae the effective coherence can be nearly as long due to wave-spreading effects [49, 51]. The DaB, however, is expected to be largely composed of incoherent waves from sources across the Universe, implying $Q \simeq \mathcal{O}(1)$. This is also the case for the cosmic axion background [18–20]. These effects may pose challenges for direct detection, and call for further investigations.

We further stress that the distribution of axion energies in the DaB can encode unique information about the cosmological distribution of sources, see Fig. 4. In the event of a successful cold axion DM detection, a dedicated DaB search carries the potential to unlock substantial novel information related to the cosmological production, SM couplings, and self-interactions of axions. We leave detailed study of these topics for future work.

7 Conclusions

While conventional axion searches have primarily focused on cold axions constituting DM, relativistic axions offer novel rich opportunities to probe fundamental physics and theories. We have developed a general framework to describe DaB formed from accumulation of emitted relativistic axions from populations of distinct historic transient sources. Utilizing a small number of key input parameters that describe the cosmological population and emission properties of the sources, depending on the theory, our framework allows to easily extract the energy density and flux of the resulting axions in the vicinity of terrestrial and space-based experiments. We show that our analysis allows to comprehensively and systematically explore a wide range of DaB sources, include those related to astrophysics such as supernovae or NS mergers, as well as originating from dark sector dynamics such as axion star bosonova explosions.

For axions coupled to photons, we established sensitive constraints on the DaB flux associated with light axions of mass $m \lesssim 10^{-3}$ eV originating from energetic sources with $\omega \gtrsim$ MeV considering axion-photon conversion and subsequent photon detection within a range of experiments such as COMPTEL, NuSTAR, XMM-Newton, INTEGRAL, EGRET and Fermi. We demonstrate that future experiments, including SKA, JWST, XRISM, Vera C. Rubin Observatory and AMEGO/e-ASTROGAM have the capability to probe axion-photon couplings with remarkable sensitivity over multiple orders of magnitude in parameter space in axion masses and couplings for sources emitting axions with energies as low as 0.1 μ eV.

Focusing on relativistic axion bursts originating during or after structure formation $z \lesssim 20$, we find that the details of the cosmological burst history in this parameter range play a less significant role than the total converted fraction \mathcal{F} and the axion emission spectrum $dN_a/d\omega$, which largely drive the size and detection sensitivity of signals. This allows to derive strong constraints from non-observation of photons from the DaB that largely do not significantly rely on cosmological assumptions. In the event of a detection, the spectrum of the DaB could provide detailed information on the cosmological evolution of axions and properties of the emission sources. When the axion emission bursts primarily occur within a short period at

redshift $z > 1$, the flux can exceed the expected background flux from local DM, providing novel prospects for both direct and indirect detection that are worthy of further exploration.

Other DaB searches offer additional prospects and opportunities to probe theories beyond SM. In particular, different signatures, such as novel extragalactic γ -ray background contributions, can appear from non-photon axion couplings, motivating further analyses. Direct detection of DaB will manifest distinctly from cold axion DM and is complementary to direct searches of relativistic axions from individual transient events.

We demonstrated that a broad variety of distinct sources can contribute to DaB , offering rich prospects for studying new physics. Many relativistic axion emission mechanisms and resulting axion emission flux sources, as well as their cosmological population distributions and statistics remain poorly understood. Our work highlights the necessity and serves as an impetus calling for detailed numerical studies and simulations required to systematically describe and quantify these scenarios.

Acknowledgements

We would like to thank Jason Arakawa, John Beacom, Oindrila Ghosh, Shunsaku Horiuchi, Marianna Safronova, and Muhammad Zaheer for discussions, as well as Pierluca Carenza and Hyungjin Kim for comments on an early draft. The work of JE was supported by the World Premier International Research Center Initiative (WPI), MEXT, Japan and by the JSPS KAKENHI Grant Numbers 21H05451 and 21K20366, as well as by the Swedish Research Council (VR) under grants 2018-03641 and 2019-02337. VT acknowledges support by the World Premier International Research Center Initiative (WPI), MEXT, Japan and JSPS KAKENHI grant No. 23K13109. This article is based upon work from COST Action COSMIC WISPerS CA21106, supported by COST (European Cooperation in Science and Technology). We acknowledge the use of the AxionLimits on GitHub [223] for compilation of existing constraints.

A Results for different cosmological rate functions

In the main text we analyzed DaB detection sensitivity for a power-law rate distribution (see Eq. (2.7)) of cosmological transient sources, considering $z_{\max} = 20$ and power-law exponent $p = -1$. Here, we show results for different cosmological assumptions, finding similar features. In Fig. 15 we display the photon flux associated with magnetic field conversion as well as decays of axions from DaB as in Fig. 7 (upper panel) and Fig. 8 (lower), but considering sources distributed according to power-law rate function with an exponent of $p = 1$ (blue lines) and $p = -3$ (red). We observe that the change in exponent modifies distribution of energies, with larger p implying a greater fraction of the flux lying at lower energies. Fig. 16 illustrates the photon flux from DaB for sources distributed according to Gaussian rate function with $\bar{z} = 5$ (red lines) and $\bar{z} = 15$ (black), which is more peaked than in the power-law case.

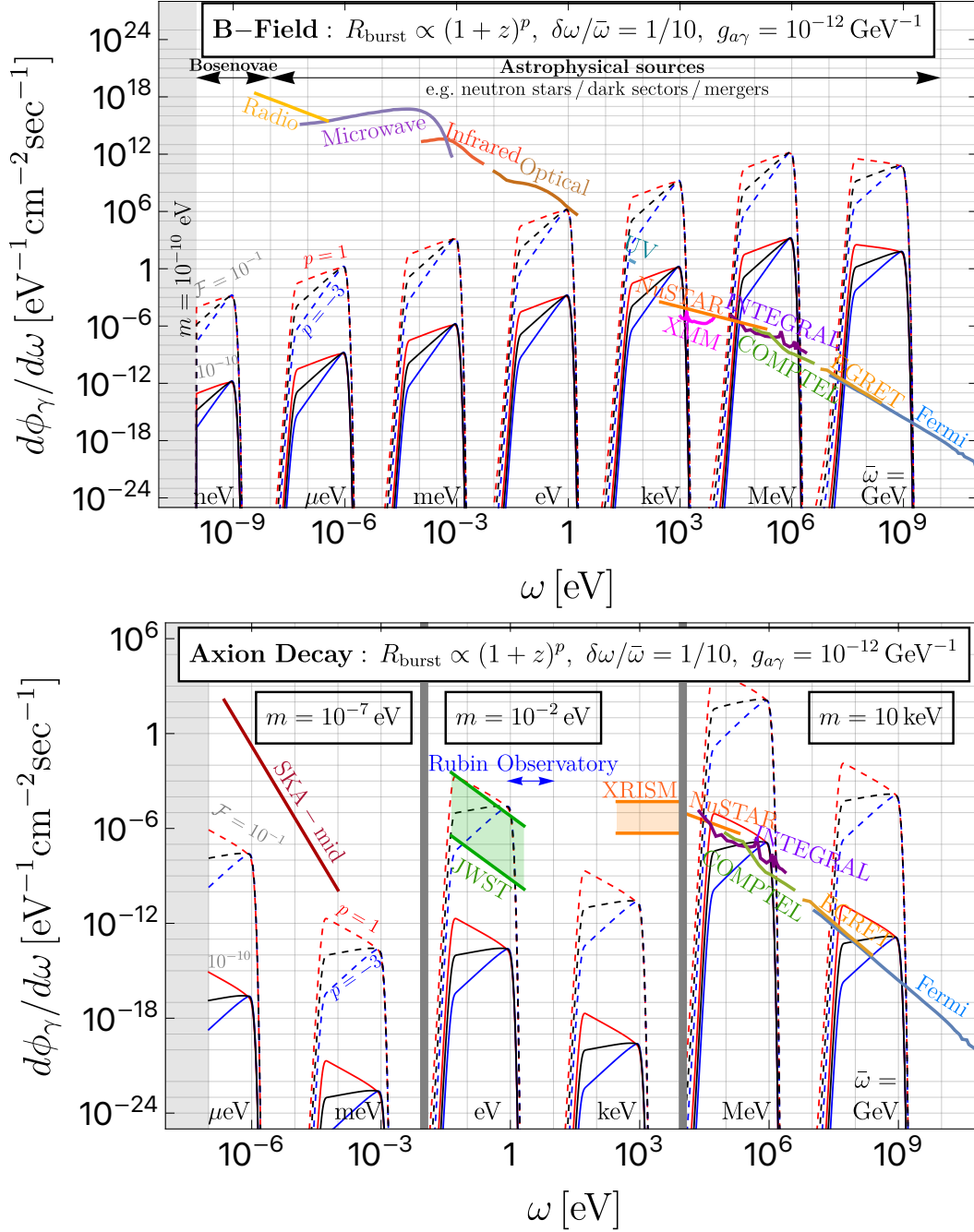


Figure 15: Analogous to Fig. 7 (upper) and Fig. 8 (lower), but considering DaB arises from transient sources with cosmological burst rate of power-law with exponent $p = 1$ (red) and $p = -3$ (blue) in addition to $p = -1$ (black), $R_{\text{burst}} \propto (1+z)^p$. For B -field conversion we take $R = \text{kpc}$, and for axion decay we assume a typical source distance of $R(z_{\text{eff}}) \simeq 1/H(z_{\text{eff}})$ with z_{eff} given by Eq. (3.12) for different values of p .

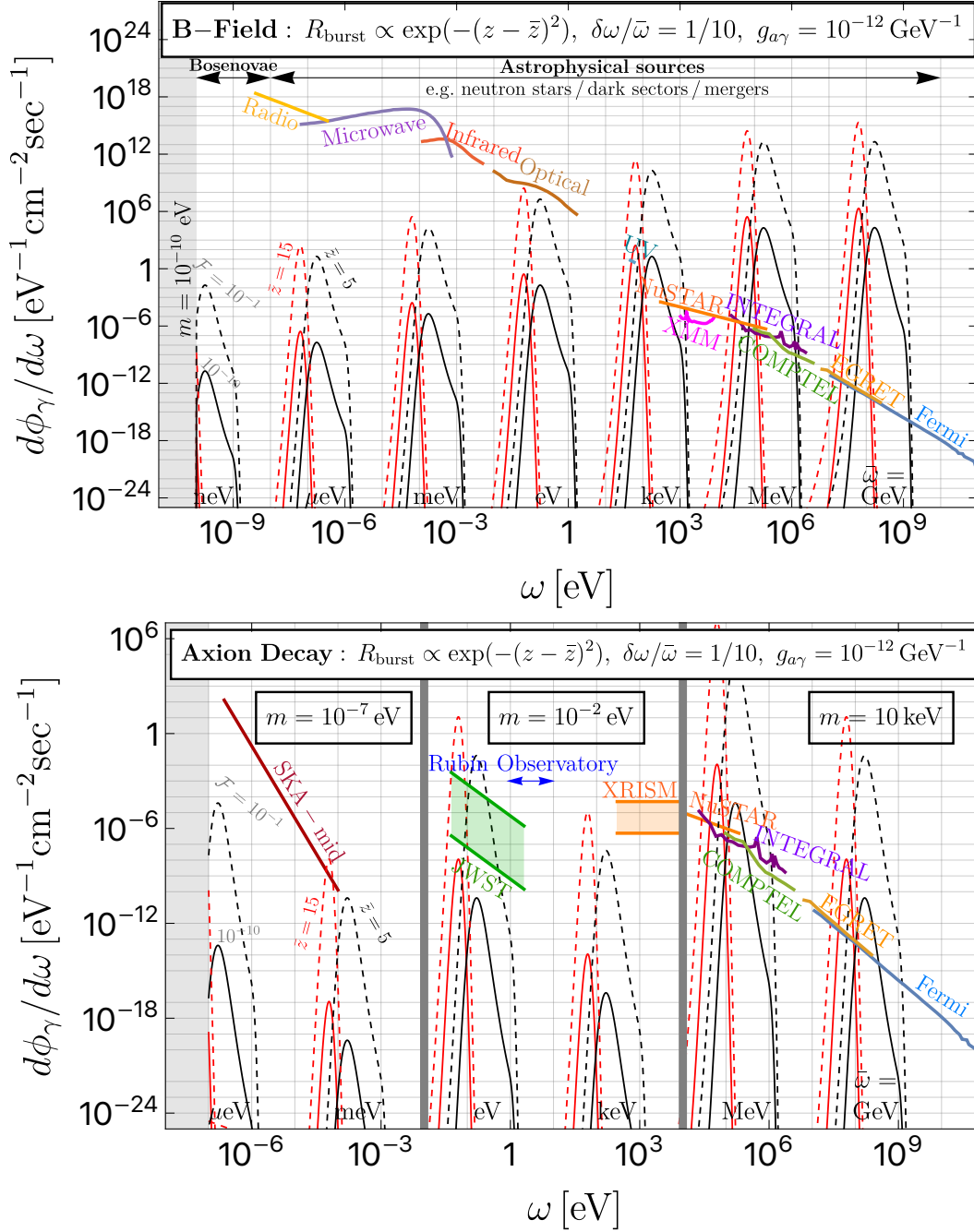


Figure 16: Analogous to Fig. 7 (upper) and Fig. 8 (lower), but considering DaB arises from transient sources with cosmological burst rate of gaussian with width $\delta z = 1$ and mean $\bar{z} = 5$ (red) and $\bar{z} = 15$ (black), $R_{\text{burst}} \propto \exp(-(z - \bar{z})^2/\delta z^2)$. For B -field conversion we take $R = \text{kpc}$, and for axion decay we assume a typical source distance of $R(z_{\text{eff}}) \simeq 1/H(z_{\text{eff}})$ with z_{eff} given by Eq. (3.12).

In Fig. 17, we display sensitivity to DaB as in Fig. 9 and Fig. 12, but considering a power-law distribution of transient sources with a different exponent parameter of $p = 1$. While the sensitivity estimates are seen to be modified, our conclusions regarding the reach of present and future searches are not significantly affected. We also repeat our analysis using a Gaussian distribution of axion emission sources as described by Eq. (2.7), with peak at $z = \bar{z}$ and spread δz . The sensitivity estimates for this case are shown in Fig. 18 and Fig. 19 for $\bar{z} = 5$ and $\bar{z} = 15$, respectively. In both cases we consider $\delta z = 1$, noting that that our results do not depend sensitively on this choice. Importantly, the peak of the energy spectrum is always located at $\bar{\omega}/(1 + \bar{z})$, hence the same experiments can be utilized to search for high-redshift (i.e. $\bar{z} \gg 1$) sources. The detection of a peaked signal originating at \bar{z} would be optimized if the search occurs near energies of order $\bar{\omega}/(1 + \bar{z})$.

B Photon flux estimates for future experiments

Here, we briefly summarize considerations for estimating differential flux $d\phi_\gamma/d\omega$ sensitivity of future experiments as shown in e.g. Fig. 10. These results highlight their significant potential to probe a wide range of DaB contributions.

Square Kilometer Array (SKA) [183–185]: the signal and noise flux is estimated as described in Sec. 4.2.

Vera C. Rubin Observatory (Rubin, formerly LSST) [176, 177]: the expected range of sensitivity to photon energy between (1 – 10) eV is shown, without detailed sensitivity estimate.

James Webb Space Telescope (JWST) [178–181]: the expected JWST background spectrum for Galactic Center observations with polar angle $\theta_{GC} = 10^\circ$ and 45° are shown in supplemental material of Ref. [181]. Fig. S3, depicts that while the two differ in detail, both lie in the range $\mathcal{B} = (0.1 - 10^3)\text{MJy} = 6.2 \cdot (10^{-19} - 10^{-15})\text{eV/cm}^2$ for wavelengths $\lambda = (0.6 - 29)\mu\text{m}$, which corresponds to energy range $\omega = (0.04 - 2)\text{eV}$. Considering this estimate along with a total observing time of $t_{\text{JWST}} = 10^3\text{sec}$ (see Tab. 1), we calculate conversion $\mathcal{B} \simeq t_{\text{JWST}}\omega^2 d\phi_\gamma/d\omega$ to generate results shown in Fig. 7.

X-Ray Imaging and Spectroscopy Mission (XRISM) [182]: simulated spectrum for XRISM observations of the core of M87 (Virgo A) galaxy can be found in Fig. 7 of Ref. [182], which gives $\mathcal{C} = (0.1 - 10)\text{counts/keV/s}$ in the energy range 0.3 – 10 keV. The effective collecting area in XRISM is reported to be $> 160\text{cm}^2$ at 1 keV and $> 210\text{cm}^2$ at 6 keV [245]. For our estimates, we consider an area of $A = 200\text{cm}^2$. To translate the relevant quantities to units of Fig. 10, we use $\mathcal{C} \simeq A d\phi_\gamma/d\omega$.

All-sky Medium Energy Gamma-ray Observatory (AMEGO) and A space mission for MeV-GeV gamma-ray astrophysics (e-ASTROGAM) [217–220]: These distinct proposals for MeV-energy gamma-ray search experiments have been estimated to have similar sensitivity, prompting us to consider them together. Estimate of the sensitivity of ASTROMEVO of $\mathcal{S} \simeq (2 - 4) \cdot 10^{-12}\text{erg cm}^{-2}\text{s}^{-1}$ in the photon energy range $\omega = (0.1 - 300)\text{MeV}$ can be found in Fig. 1 of Ref. [218]. We use the relation $\mathcal{S} \simeq \omega^2 d\phi_\gamma/d\omega$ to convert this into flux employed

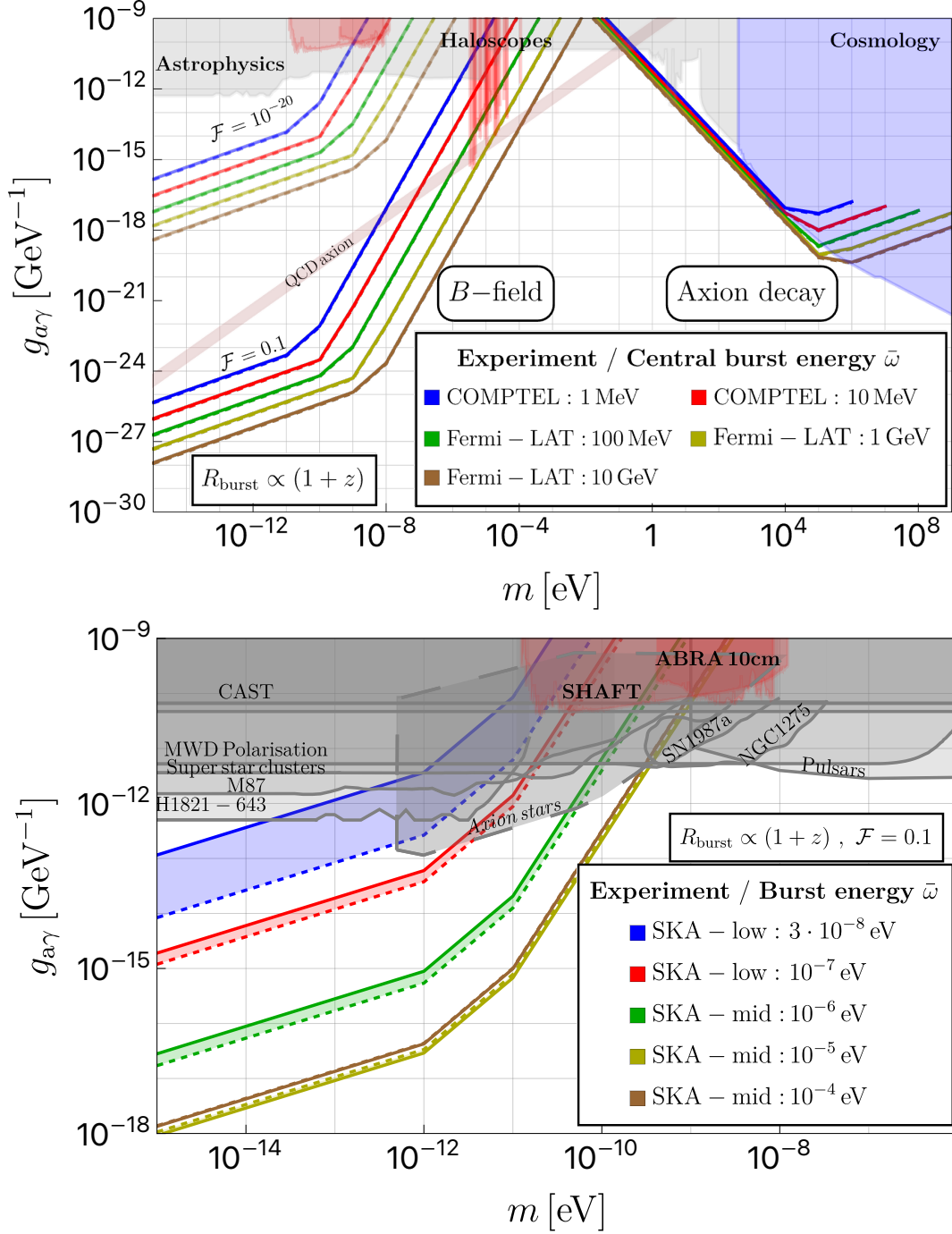


Figure 17: Analogous to Fig. 9 (upper) and Fig. 12 (lower), but considering DaB arises from transient sources with cosmological burst rate of power-law with exponent $p = 1$, $R_{\text{burst}} \propto (1+z)$. For B -field conversion we take $R = \text{kpc}$, and for axion decay we assume a typical source distance of $R(z_{\text{eff}}) \simeq 1/H(z_{\text{eff}})$ with $z_{\text{eff}} \simeq 2/5$.

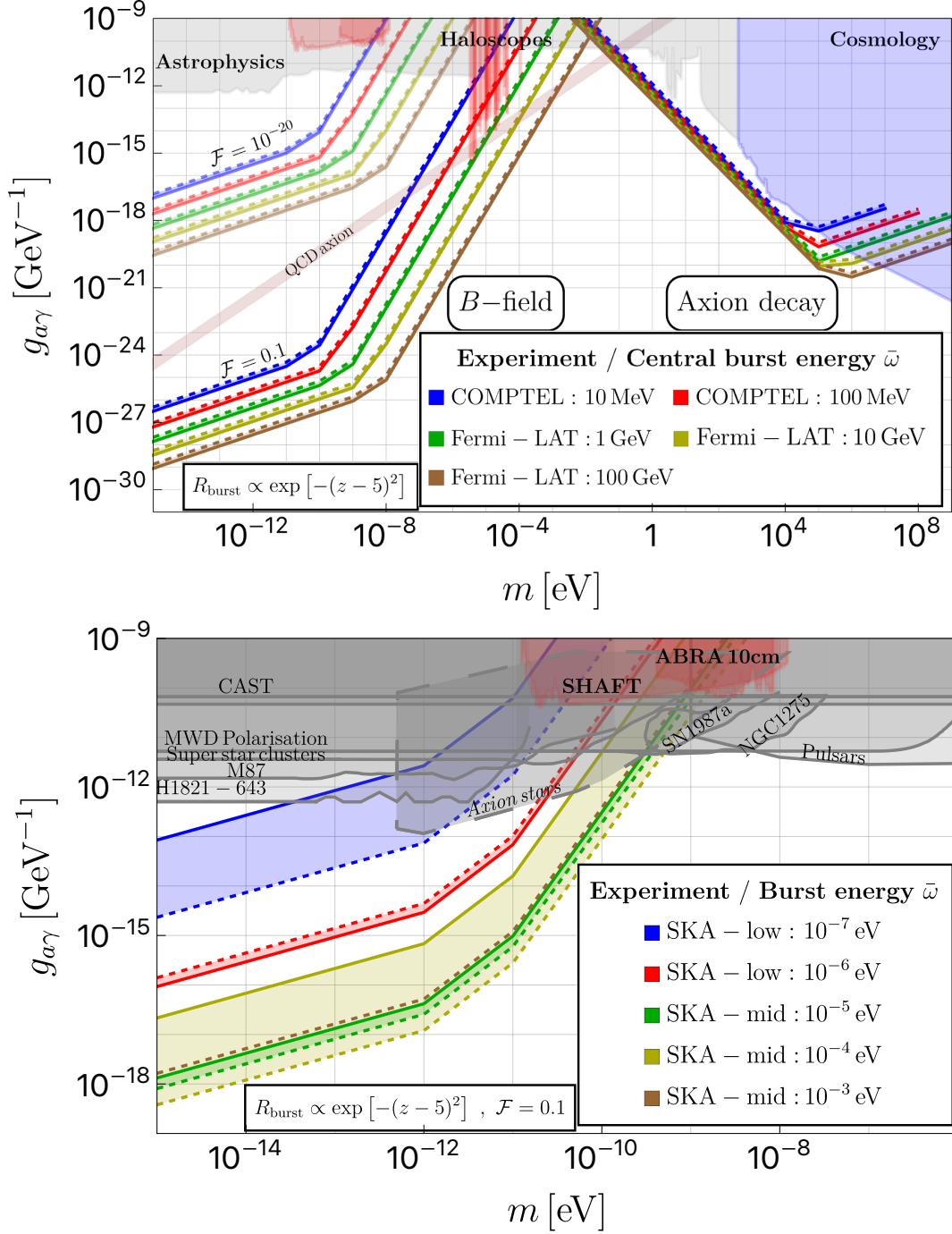


Figure 18: Analogous to Fig. 9 (upper) and Fig. 12 (lower), but using a Gaussian cosmological transient rate function $f(z) = \exp[-(z - \bar{z})^2/\delta z^2]$ instead of a power law. For B -field conversion we take $R = \text{kpc}$, and for axion decay we assume a typical source distance of $R(z_{\text{eff}}) \simeq 1/H(z_{\text{eff}})$ with z_{eff} given by Eq. (3.12). Here, we set $\bar{z} = 5$ and $\delta z = 1$.

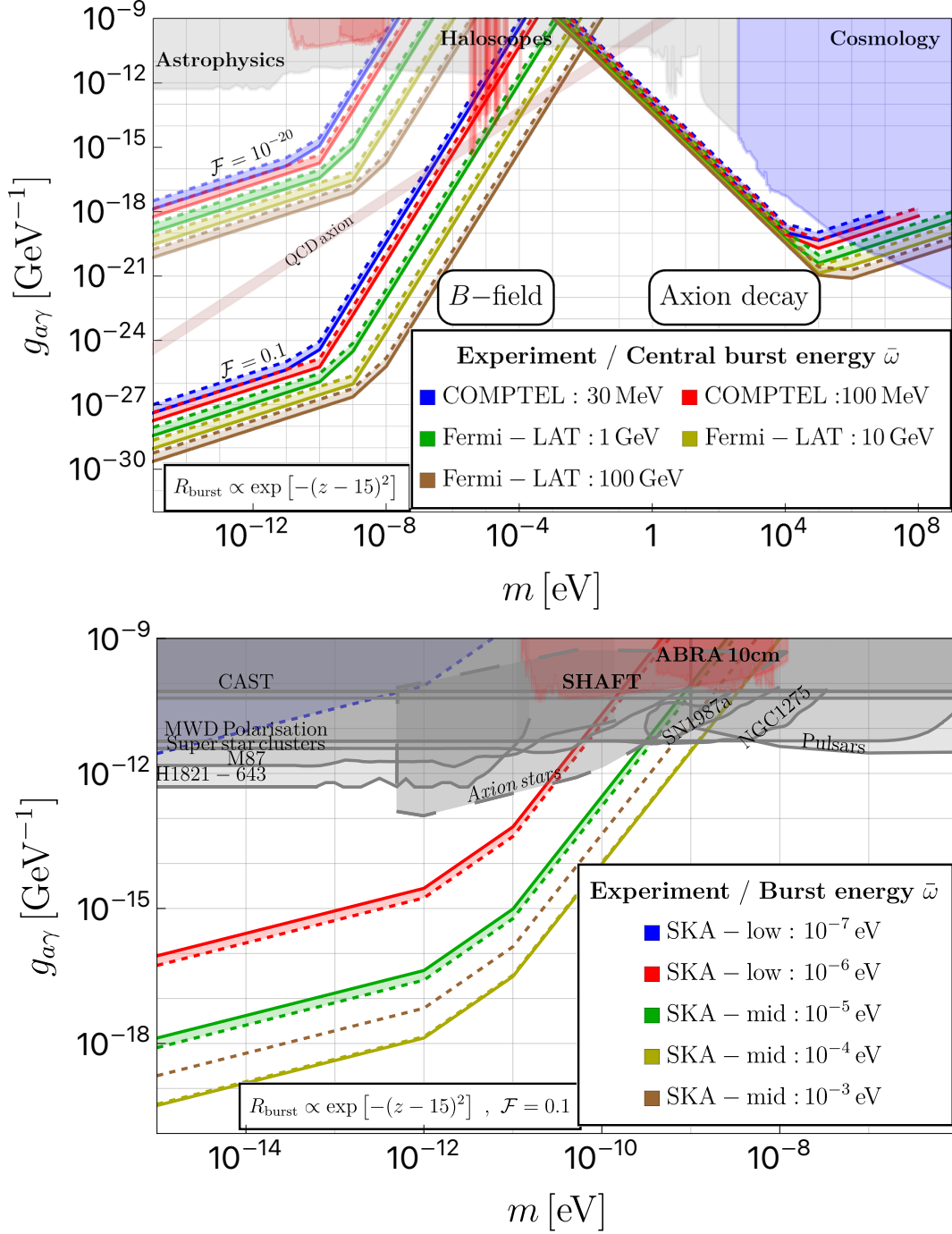


Figure 19: Analogous to Fig. 9 (upper) and Fig. 12 (lower), but using a Gaussian cosmological transient rate function $f(z) = \exp[-(z - \bar{z})^2/\delta z^2]$ rather than a power law. For B -field conversion we take $R = \text{kpc}$, and for axion decay we assume a typical source distance of $R(z_{\text{eff}}) \simeq 1/H(z_{\text{eff}})$ with z_{eff} given by Eq. (3.12). Here, we set $\bar{z} = 15$ and $\delta z = 1$.

in Fig. 10. A more detailed sensitivity estimate for e-ASTROGAM is given in Ref. [219] (see e.g. their Fig. 8), which agrees with the above within approximately a factor of two. See also discussion of Ref. [220].

References

- [1] ATLAS collaboration, G. Aad et al., *Observation of a new particle in the search for the Standard Model Higgs boson with the ATLAS detector at the LHC*, *Phys. Lett. B* **716** (2012) 1 [1207.7214].
- [2] CMS collaboration, S. Chatrchyan et al., *Observation of a New Boson at a Mass of 125 GeV with the CMS Experiment at the LHC*, *Phys. Lett. B* **716** (2012) 30 [1207.7235].
- [3] R. Peccei and H. R. Quinn, *CP Conservation in the Presence of Instantons*, *Phys. Rev. Lett.* **38** (1977) 1440.
- [4] S. Weinberg, *A New Light Boson?*, *Phys. Rev. Lett.* **40** (1978) 223.
- [5] F. Wilczek, *Problem of Strong P and T Invariance in the Presence of Instantons*, *Phys. Rev. Lett.* **40** (1978) 279.
- [6] J. E. Kim, *Weak Interaction Singlet and Strong CP Invariance*, *Phys. Rev. Lett.* **43** (1979) 103.
- [7] M. A. Shifman, A. Vainshtein and V. I. Zakharov, *Can Confinement Ensure Natural CP Invariance of Strong Interactions?*, *Nucl. Phys. B* **166** (1980) 493.
- [8] A. Zhitnitsky, *On Possible Suppression of the Axion Hadron Interactions. (In Russian)*, *Sov. J. Nucl. Phys.* **31** (1980) 260.
- [9] M. Dine, W. Fischler and M. Srednicki, *A Simple Solution to the Strong CP Problem with a Harmless Axion*, *Phys. Lett. B* **104** (1981) 199.
- [10] J. Preskill, M. B. Wise and F. Wilczek, *Cosmology of the Invisible Axion*, *Phys. Lett. B* **120** (1983) 127.
- [11] L. Abbott and P. Sikivie, *A Cosmological Bound on the Invisible Axion*, *Phys. Lett. B* **120** (1983) 133.
- [12] M. Dine and W. Fischler, *The Not So Harmless Axion*, *Phys. Lett. B* **120** (1983) 137.
- [13] P. Svrcek and E. Witten, *Axions In String Theory*, *JHEP* **06** (2006) 051 [hep-th/0605206].
- [14] A. Arvanitaki, S. Dimopoulos, S. Dubovsky, N. Kaloper and J. March-Russell, *String Axiverse*, *Phys. Rev. D* **81** (2010) 123530 [0905.4720].
- [15] I. G. Irastorza and J. Redondo, *New experimental approaches in the search for axion-like particles*, *Prog. Part. Nucl. Phys.* **102** (2018) 89 [1801.08127].
- [16] P. Agrawal et al., *Feebly-interacting particles: FIPs 2020 workshop report*, *Eur. Phys. J. C* **81** (2021) 1015 [2102.12143].
- [17] C. B. Adams et al., *Axion Dark Matter*, in *Snowmass 2021*, 3, 2022, 2203.14923.
- [18] J. P. Conlon and M. C. D. Marsh, *The Cosmophenomenology of Axionic Dark Radiation*, *JHEP* **10** (2013) 214 [1304.1804].

- [19] M. C. D. Marsh, *Hints of a Cosmic Axion Background*, in *9th Patras Workshop on Axions, WIMPs and WISPs*, pp. 159–163, 2013, [DOI](#).
- [20] J. A. Dror, H. Murayama and N. L. Rodd, *Cosmic axion background*, *Phys. Rev. D* **103** (2021) 115004 [[2101.09287](#)].
- [21] M. S. Turner, *Thermal Production of Not SO Invisible Axions in the Early Universe*, *Phys. Rev. Lett.* **59** (1987) 2489.
- [22] S. Chang and K. Choi, *Hadronic axion window and the big bang nucleosynthesis*, *Phys. Lett. B* **316** (1993) 51 [[hep-ph/9306216](#)].
- [23] E. Masso, F. Rota and G. Zsembinski, *On axion thermalization in the early universe*, *Phys. Rev. D* **66** (2002) 023004 [[hep-ph/0203221](#)].
- [24] S. Hannestad, A. Mirizzi and G. Raffelt, *New cosmological mass limit on thermal relic axions*, *JCAP* **07** (2005) 002 [[hep-ph/0504059](#)].
- [25] P. Graf and F. D. Steffen, *Thermal axion production in the primordial quark-gluon plasma*, *Phys. Rev. D* **83** (2011) 075011 [[1008.4528](#)].
- [26] A. Salvio, A. Strumia and W. Xue, *Thermal axion production*, *JCAP* **01** (2014) 011 [[1310.6982](#)].
- [27] F. Arias-Aragón, F. D’Eramo, R. Z. Ferreira, L. Merlo and A. Notari, *Production of Thermal Axions across the ElectroWeak Phase Transition*, *JCAP* **03** (2021) 090 [[2012.04736](#)].
- [28] E. J. Chun and A. Lukas, *Axino mass in supergravity models*, *Phys. Lett. B* **357** (1995) 43 [[hep-ph/9503233](#)].
- [29] T. Asaka and M. Yamaguchi, *Hadronic axion model in gauge mediated supersymmetry breaking and cosmology of saxion*, *Phys. Rev. D* **59** (1999) 125003 [[hep-ph/9811451](#)].
- [30] K. Ichikawa, M. Kawasaki, K. Nakayama, M. Senami and F. Takahashi, *Increasing effective number of neutrinos by decaying particles*, *JCAP* **05** (2007) 008 [[hep-ph/0703034](#)].
- [31] M. Kawasaki, K. Nakayama and M. Senami, *Cosmological implications of supersymmetric axion models*, *JCAP* **03** (2008) 009 [[0711.3083](#)].
- [32] S. Kasuya, M. Kawasaki and T. Yanagida, *Cosmological axion problem in chaotic inflationary universe*, *Phys. Lett. B* **409** (1997) 94 [[hep-ph/9608405](#)].
- [33] Y. Ema and K. Nakayama, *Explosive Axion Production from Saxion*, *Phys. Lett. B* **776** (2018) 174 [[1710.02461](#)].
- [34] R. T. Co, L. J. Hall and K. Harigaya, *QCD Axion Dark Matter with a Small Decay Constant*, *Phys. Rev. Lett.* **120** (2018) 211602 [[1711.10486](#)].
- [35] G. G. Raffelt, *Stars as laboratories for fundamental physics: The astrophysics of neutrinos, axions, and other weakly interacting particles*. 5, 1996.
- [36] P. Sikivie, *Experimental Tests of the Invisible Axion*, *Phys. Rev. Lett.* **51** (1983) 1415.
- [37] S. Moriyama, *A Proposal to search for a monochromatic component of solar axions using Fe-57*, *Phys. Rev. Lett.* **75** (1995) 3222 [[hep-ph/9504318](#)].
- [38] J. Eby, M. Leembruggen, P. Suranyi and L. C. R. Wijewardhana, *Collapse of Axion Stars*, *JHEP* **12** (2016) 066 [[1608.06911](#)].

- [39] D. G. Levkov, A. G. Panin and I. I. Tkachev, *Relativistic axions from collapsing Bose stars*, *Phys. Rev. Lett.* **118** (2017) 011301 [[1609.03611](#)].
- [40] A. Arvanitaki and S. Dubovsky, *Exploring the String Axiverse with Precision Black Hole Physics*, *Phys. Rev. D* **83** (2011) 044026 [[1004.3558](#)].
- [41] A. Arvanitaki, M. Baryakhtar and X. Huang, *Discovering the QCD Axion with Black Holes and Gravitational Waves*, *Phys. Rev. D* **91** (2015) 084011 [[1411.2263](#)].
- [42] A. Arvanitaki, M. Baryakhtar, S. Dimopoulos, S. Dubovsky and R. Lasenby, *Black Hole Mergers and the QCD Axion at Advanced LIGO*, *Phys. Rev. D* **95** (2017) 043001 [[1604.03958](#)].
- [43] M. Baryakhtar, M. Galanis, R. Lasenby and O. Simon, *Black hole superradiance of self-interacting scalar fields*, *Phys. Rev. D* **103** (2021) 095019 [[2011.11646](#)].
- [44] C. Ünal, F. Pacucci and A. Loeb, *Properties of ultralight bosons from heavy quasar spins via superradiance*, *JCAP* **05** (2021) 007 [[2012.12790](#)].
- [45] N. P. Branco, R. Z. Ferreira and J. a. G. Rosa, *Superradiant axion clouds around asteroid-mass primordial black holes*, *JCAP* **04** (2023) 003 [[2301.01780](#)].
- [46] A. Banerjee, D. Budker, J. Eby, H. Kim and G. Perez, *Relaxion Stars and their detection via Atomic Physics*, *Commun. Phys.* **3** (2020) 1 [[1902.08212](#)].
- [47] A. Banerjee, D. Budker, J. Eby, V. V. Flambaum, H. Kim, O. Matsedonskyi et al., *Searching for Earth/Solar Axion Halos*, *JHEP* **09** (2020) 004 [[1912.04295](#)].
- [48] D. Budker, J. Eby, M. Gorghetto, M. Jiang and G. Perez, *A Generic Formation Mechanism of Ultralight Dark Matter Solar Halos*, [2306.12477](#).
- [49] J. Eby, S. Shirai, Y. V. Stadnik and V. Takhistov, *Probing relativistic axions from transient astrophysical sources*, *Phys. Lett. B* **825** (2022) 136858 [[2106.14893](#)].
- [50] S. Chigusa, A. Ito, K. Nakayama and V. Takhistov, *Effects of Finite Material Size On Axion-magnon Conversion*, [2310.17704](#).
- [51] J. Arakawa, J. Eby, M. S. Safronova, V. Takhistov and M. H. Zaheer, *Detection of Bosonovae with Quantum Sensors on Earth and in Space*, [2306.16468](#).
- [52] C. Dailey, C. Bradley, D. F. Jackson Kimball, I. A. Sulai, S. Pustelny, A. Wickenbrock et al., *Quantum sensor networks as exotic field telescopes for multi-messenger astronomy*, *Nature Astron.* **5** (2021) 150 [[2002.04352](#)].
- [53] G. G. Raffelt, J. Redondo and N. Viaux Maira, *The meV mass frontier of axion physics*, *Phys. Rev. D* **84** (2011) 103008 [[1110.6397](#)].
- [54] F. Calore, P. Carena, M. Giannotti, J. Jaeckel and A. Mirizzi, *Bounds on axionlike particles from the diffuse supernova flux*, *Phys. Rev. D* **102** (2020) 123005 [[2008.11741](#)].
- [55] F. Calore, P. Carena, C. Eckner, T. Fischer, M. Giannotti, J. Jaeckel et al., *3D template-based Fermi-LAT constraints on the diffuse supernova axion-like particle background*, *Phys. Rev. D* **105** (2022) 063028 [[2110.03679](#)].
- [56] V. Takhistov, *Neutrino and Axion Astronomy with Dark Matter Experiments*, *J. Phys. Conf. Ser.* **2156** (2021) 012049 [[2111.04088](#)].

- [57] J. F. Beacom, *The Diffuse Supernova Neutrino Background*, *Ann. Rev. Nucl. Part. Sci.* **60** (2010) 439 [1004.3311].
- [58] S. Horiuchi, J. F. Beacom and E. Dwek, *The Diffuse Supernova Neutrino Background is detectable in Super-Kamiokande*, *Phys. Rev. D* **79** (2009) 083013 [0812.3157].
- [59] SUPER-KAMIOKANDE collaboration, K. Abe et al., *Diffuse supernova neutrino background search at Super-Kamiokande*, *Phys. Rev. D* **104** (2021) 122002 [2109.11174].
- [60] X.-D. Shi and G. M. Fuller, *Neutrinos and supermassive stars: Prospects for neutrino emission and detection*, *Astrophys. J.* **503** (1998) 307 [astro-ph/9801106].
- [61] F. Linke, J. A. Font, H.-T. Janka, E. Muller and P. Papadopoulos, *Spherical collapse of supermassive stars: Neutrino emission and gamma-ray bursts*, *Astron. Astrophys.* **376** (2001) 568 [astro-ph/0103144].
- [62] V. Munoz, V. Takhistov, S. J. Witte and G. M. Fuller, *Exploring the origin of supermassive black holes with coherent neutrino scattering*, *JCAP* **11** (2021) 020 [2102.00885].
- [63] J. P. Conlon and M. C. D. Marsh, *Excess Astrophysical Photons from a 0.1–1 keV Cosmic Axion Background*, *Phys. Rev. Lett.* **111** (2013) 151301 [1305.3603].
- [64] S. Angus, J. P. Conlon, M. C. D. Marsh, A. J. Powell and L. T. Witkowski, *Soft X-ray Excess in the Coma Cluster from a Cosmic Axion Background*, *JCAP* **09** (2014) 026 [1312.3947].
- [65] J. Jaeckel and W. Yin, *Shining ALP dark radiation*, *Phys. Rev. D* (2022) 115003 [2110.03692].
- [66] Y. Cui, J.-L. Kuo, J. Pradler and Y.-D. Tsai, *Shining light on cosmogenic axions with neutrino experiments*, *Phys. Rev. D* **106** (2022) 115024 [2207.13107].
- [67] A. Kar, T. Kumar, S. Roy and J. Zupan, *Searching for relativistic axions in the sky*, *JCAP* **08** (2023) 056 [2212.04647].
- [68] ADMX collaboration, T. Nitta et al., *Search for a Dark-Matter-Induced Cosmic Axion Background with ADMX*, *Phys. Rev. Lett.* **131** (2023) 101002 [2303.06282].
- [69] S. Ando, N. Ekanger, S. Horiuchi and Y. Koshio, *Diffuse neutrino background from past core-collapse supernovae*, 6, 2023, 2306.16076.
- [70] X.-D. Shi, G. M. Fuller and F. Halzen, *Observing the birth of supermassive black holes with the ‘ICECUBE’ neutrino detector*, *Phys. Rev. Lett.* **81** (1998) 5722 [astro-ph/9805242].
- [71] PLANCK collaboration, N. Aghanim et al., *Planck 2018 results. VI. Cosmological parameters*, *Astron. Astrophys.* **641** (2020) A6 [1807.06209].
- [72] P. Carena, T. Fischer, M. Giannotti, G. Guo, G. Martínez-Pinedo and A. Mirizzi, *Improved axion emissivity from a supernova via nucleon-nucleon bremsstrahlung*, *JCAP* **10** (2019) 016 [1906.11844].
- [73] P. Carena, B. Fore, M. Giannotti, A. Mirizzi and S. Reddy, *Enhanced Supernova Axion Emission and its Implications*, *Phys. Rev. Lett.* **126** (2021) 071102 [2010.02943].
- [74] A. Lella, P. Carena, G. Lucente, M. Giannotti and A. Mirizzi, *Protoneutron stars as cosmic factories for massive axionlike particles*, *Phys. Rev. D* **107** (2023) 103017 [2211.13760].
- [75] N. H. Nguyen, E. H. Tanin and M. Kamionkowski, *Spectra of axions emitted from main sequence stars*, *JCAP* **11** (2023) 091 [2307.11216].

- [76] S. P. Harris, J.-F. Fortin, K. Sinha and M. G. Alford, *Axions in neutron star mergers*, *JCAP* **07** (2020) 023 [[2003.09768](#)].
- [77] D. F. G. Fiorillo and F. Iocco, *Axions from neutron star mergers*, *Phys. Rev. D* **105** (2022) 123007.
- [78] G. G. Raffelt, *Astrophysical methods to constrain axions and other novel particle phenomena*, *Phys. Rept.* **198** (1990) 1.
- [79] G. G. Raffelt, *Astrophysical axion bounds*, *Lect. Notes Phys.* **741** (2008) 51 [[hep-ph/0611350](#)].
- [80] T. Fischer, S. Chakraborty, M. Giannotti, A. Mirizzi, A. Payez and A. Ringwald, *Probing axions with the neutrino signal from the next galactic supernova*, *Phys. Rev. D* **94** (2016) 085012 [[1605.08780](#)].
- [81] A. Caputo and G. Raffelt, *Astrophysical Axion Bounds: The 2024 Edition*, in *1st Training School of the COST Action COSMIC WISPerS (CA21106)*, 1, 2024, [2401.13728](#).
- [82] KAMIOKANDE-II collaboration, K. Hirata et al., *Observation of a Neutrino Burst from the Supernova SN 1987a*, *Phys. Rev. Lett.* **58** (1987) 1490.
- [83] R. M. Bionta et al., *Observation of a Neutrino Burst in Coincidence with Supernova SN 1987a in the Large Magellanic Cloud*, *Phys. Rev. Lett.* **58** (1987) 1494.
- [84] E. N. Alekseev, L. N. Alekseeva, I. V. Krivosheina and V. I. Volchenko, *Detection of the Neutrino Signal From SN1987A in the LMC Using the Inr Baksan Underground Scintillation Telescope*, *Phys. Lett. B* **205** (1988) 209.
- [85] M. S. Turner, *Axions from SN 1987a*, *Phys. Rev. Lett.* **60** (1988) 1797.
- [86] A. Burrows, M. S. Turner and R. P. Brinkmann, *Axions and SN 1987a*, *Phys. Rev. D* **39** (1989) 1020.
- [87] A. Burrows, M. T. Ressel and M. S. Turner, *Axions and SN1987A: Axion trapping*, *Phys. Rev. D* **42** (1990) 3297.
- [88] G. Raffelt and D. Seckel, *Bounds on Exotic Particle Interactions from SN 1987a*, *Phys. Rev. Lett.* **60** (1988) 1793.
- [89] W. Keil, H.-T. Janka, D. N. Schramm, G. Sigl, M. S. Turner and J. R. Ellis, *A Fresh look at axions and SN-1987A*, *Phys. Rev. D* **56** (1997) 2419 [[astro-ph/9612222](#)].
- [90] C. Hanhart, D. R. Phillips and S. Reddy, *Neutrino and axion emissivities of neutron stars from nucleon-nucleon scattering data*, *Phys. Lett. B* **499** (2001) 9 [[astro-ph/0003445](#)].
- [91] J. H. Chang, R. Essig and S. D. McDermott, *Supernova 1987A Constraints on Sub-GeV Dark Sectors, Millicharged Particles, the QCD Axion, and an Axion-like Particle*, *JHEP* **09** (2018) 051 [[1803.00993](#)].
- [92] G. G. Raffelt, *ASTROPHYSICAL AXION BOUNDS DIMINISHED BY SCREENING EFFECTS*, *Phys. Rev. D* **33** (1986) 897.
- [93] J. Jaeckel and A. Ringwald, *The Low-Energy Frontier of Particle Physics*, *Ann. Rev. Nucl. Part. Sci.* **60** (2010) 405 [[1002.0329](#)].
- [94] A. Caputo, G. Raffelt and E. Vitagliano, *Muonic boson limits: Supernova redux*, *Phys. Rev. D* **105** (2022) 035022 [[2109.03244](#)].

- [95] A. Caputo, G. Raffelt and E. Vitagliano, *Radiative transfer in stars by feebly interacting bosons*, *JCAP* **08** (2022) 045 [[2204.11862](#)].
- [96] A. Lella, P. Carena, G. Co', G. Lucente, M. Giannotti, A. Mirizzi et al., *Getting the most on supernova axions*, *Phys. Rev. D* **109** (2024) 023001 [[2306.01048](#)].
- [97] J. A. Grifols, E. Masso and R. Toldra, *Gamma-rays from SN1987A due to pseudoscalar conversion*, *Phys. Rev. Lett.* **77** (1996) 2372 [[astro-ph/9606028](#)].
- [98] J. W. Brockway, E. D. Carlson and G. G. Raffelt, *SN1987A gamma-ray limits on the conversion of pseudoscalars*, *Phys. Lett. B* **383** (1996) 439 [[astro-ph/9605197](#)].
- [99] A. Payez, C. Evoli, T. Fischer, M. Giannotti, A. Mirizzi and A. Ringwald, *Revisiting the SN1987A gamma-ray limit on ultralight axion-like particles*, *JCAP* **02** (2015) 006 [[1410.3747](#)].
- [100] J. Jaeckel, P. C. Malta and J. Redondo, *Decay photons from the axionlike particles burst of type II supernovae*, *Phys. Rev. D* **98** (2018) 055032 [[1702.02964](#)].
- [101] A. Caputo, P. Carena, G. Lucente, E. Vitagliano, M. Giannotti, K. Kotake et al., *Axionlike Particles from Hypernovae*, *Phys. Rev. Lett.* **127** (2021) 181102 [[2104.05727](#)].
- [102] D. J. Kaup, *Klein-Gordon Geon*, *Phys. Rev.* **172** (1968) 1331.
- [103] R. Ruffini and S. Bonazzola, *Systems of selfgravitating particles in general relativity and the concept of an equation of state*, *Phys. Rev.* **187** (1969) 1767.
- [104] J. Breit, S. Gupta and A. Zaks, *Cold bose stars*, *Physics Letters B* **140** (1984) 329 .
- [105] M. Colpi, S. Shapiro and I. Wasserman, *Boson Stars: Gravitational Equilibria of Selfinteracting Scalar Fields*, *Phys. Rev. Lett.* **57** (1986) 2485.
- [106] E. W. Kolb and I. I. Tkachev, *Axion miniclusters and Bose stars*, *Phys. Rev. Lett.* **71** (1993) 3051 [[hep-ph/9303313](#)].
- [107] B. Eggemeier and J. C. Niemeyer, *Formation and mass growth of axion stars in axion miniclusters*, *Phys. Rev. D* **100** (2019) 063528 [[1906.01348](#)].
- [108] P.-H. Chavanis, *Mass-radius relation of Newtonian self-gravitating Bose-Einstein condensates with short-range interactions: I. Analytical results*, *Phys. Rev. D* **84** (2011) 043531 [[1103.2050](#)].
- [109] P. Chavanis and L. Delfini, *Mass-radius relation of Newtonian self-gravitating Bose-Einstein condensates with short-range interactions: II. Numerical results*, *Phys. Rev. D* **84** (2011) 043532 [[1103.2054](#)].
- [110] J. Barranco and A. Bernal, *Self-gravitating system made of axions*, *Phys. Rev. D* **83** (2011) 043525 [[1001.1769](#)].
- [111] J. Eby, P. Suranyi, C. Vaz and L. Wijewardhana, *Axion Stars in the Infrared Limit*, *JHEP* **03** (2015) 080 [[1412.3430](#)].
- [112] E. D. Schiappacasse and M. P. Hertzberg, *Analysis of Dark Matter Axion Clumps with Spherical Symmetry*, *JCAP* **01** (2018) 037 [[1710.04729](#)].
- [113] E. A. Donley, N. R. Claussen, S. L. Cornish, J. L. Roberts, E. A. Cornell and C. E. Wieman, *Dynamics of collapsing and exploding bose-einstein condensates*, *Nature* **412** (2001) 295.

- [114] J. Eby, P. Suranyi and L. Wijewardhana, *The Lifetime of Axion Stars*, *Mod. Phys. Lett. A* **31** (2016) 1650090 [[1512.01709](#)].
- [115] J. Eby, M. Ma, P. Suranyi and L. Wijewardhana, *Decay of Ultralight Axion Condensates*, *JHEP* **01** (2018) 066 [[1705.05385](#)].
- [116] X. Du, D. J. E. Marsh, M. Escudero, A. Benson, D. Blas, C. K. Pooni et al., *Soliton Merger Rates and Enhanced Axion Dark Matter Decay*, [2301.09769](#).
- [117] M. Escudero, C. K. Pooni, M. Fairbairn, D. Blas, X. Du and D. J. E. Marsh, *Axion Star Explosions: A New Source for Axion Indirect Detection*, [2302.10206](#).
- [118] P. J. Fox, N. Weiner and H. Xiao, *Recurrent Axionovae and their Cosmological Constraints*, [2302.00685](#).
- [119] M. Calzà, J. March-Russell and J. a. G. Rosa, *Evaporating primordial black holes, the string axiverse, and hot dark radiation*, [2110.13602](#).
- [120] K. Agashe, J. H. Chang, S. J. Clark, B. Dutta, Y. Tsai and T. Xu, *Detecting axionlike particles with primordial black holes*, *Phys. Rev. D* **108** (2023) 023014 [[2212.11980](#)].
- [121] Y. Jho, T.-G. Kim, J.-C. Park, S. C. Park and Y. Park, *Axions from Primordial Black Holes*, [2212.11977](#).
- [122] M. Calzà, J. a. G. Rosa and F. Serrano, *Primordial black hole superradiance and evaporation in the string axiverse*, [2306.09430](#).
- [123] M. Calzà and J. a. G. Rosa, *Evaporating Kerr black holes as probes of new physics*, [2312.09261](#).
- [124] S. W. Hawking, *Black hole explosions*, *Nature* **248** (1974) 30.
- [125] D. N. Page, *Particle Emission Rates from a Black Hole: Massless Particles from an Uncharged, Nonrotating Hole*, *Phys. Rev. D* **13** (1976) 198.
- [126] J. H. MacGibbon and B. R. Webber, *Quark and gluon jet emission from primordial black holes: The instantaneous spectra*, *Phys. Rev. D* **41** (1990) 3052.
- [127] A. Arbey and J. Auffinger, *BlackHawk: A public code for calculating the Hawking evaporation spectra of any black hole distribution*, *Eur. Phys. J. C* **79** (2019) 693 [[1905.04268](#)].
- [128] A. Arbey and J. Auffinger, *Physics Beyond the Standard Model with BlackHawk v2.0*, *Eur. Phys. J. C* **81** (2021) 910 [[2108.02737](#)].
- [129] M. Chen, G. B. Gelmini, P. Lu and V. Takhistov, *Primordial Black Hole Sterile Neutrino Dark Matter Production Independent of Couplings*, [2312.12136](#).
- [130] M. Chen, G. B. Gelmini, P. Lu and V. Takhistov, *Primordial Black Hole Neutrino Dark Matter Production Independent of Couplings*, [2309.12258](#).
- [131] T. Altherr, E. Petitgirard and T. del Rio Gaztelurrutia, *Axion emission from red giants and white dwarfs*, *Astropart. Phys.* **2** (1994) 175 [[hep-ph/9310304](#)].
- [132] G. Raffelt and A. Weiss, *Red giant bound on the axion - electron coupling revisited*, *Phys. Rev. D* **51** (1995) 1495 [[hep-ph/9410205](#)].

- [133] A. H. Corsico, O. G. Benvenuto, L. G. Althaus, J. Isern and E. Garcia-Berro, *The Potential of the variable DA white dwarf G117 - B15A as a tool for fundamental physics*, *New Astron.* **6** (2001) 197 [[astro-ph/0104103](#)].
- [134] M. M. Miller Bertolami, B. E. Melendez, L. G. Althaus and J. Isern, *Revisiting the axion bounds from the Galactic white dwarf luminosity function*, *JCAP* **10** (2014) 069 [[1406.7712](#)].
- [135] N. Iwamoto, *Axion Emission from Neutron Stars*, *Phys. Rev. Lett.* **53** (1984) 1198.
- [136] J. Keller and A. Sedrakian, *Axions from cooling compact stars*, *Nucl. Phys. A* **897** (2013) 62 [[1205.6940](#)].
- [137] A. Sedrakian, *Axion cooling of neutron stars*, *Phys. Rev. D* **93** (2016) 065044 [[1512.07828](#)].
- [138] Y. Bai and C. H. de Lima, *Electrobaryonic axion: hair of neutron stars*, [2311.18794](#).
- [139] T. Dietrich and K. Clough, *Cooling binary neutron star remnants via nucleon-nucleon-axion bremsstrahlung*, *Phys. Rev. D* **100** (2019) 083005 [[1909.01278](#)].
- [140] P. S. B. Dev, J.-F. Fortin, S. P. Harris, K. Sinha and Y. Zhang, *First Constraints on the Photon Coupling of Axion-like Particles from Multimessenger Studies of the Neutron Star Merger GW170817*, [2305.01002](#).
- [141] M. Diamond, D. F. G. Fiorillo, G. Marques-Tavares, I. Tamborra and E. Vitagliano, *Multimessenger Constraints on Radiatively Decaying Axions from GW170817*, [2305.10327](#).
- [142] A. Prabhu, *Axion production in pulsar magnetosphere gaps*, *Phys. Rev. D* **104** (2021) 055038 [[2104.14569](#)].
- [143] D. Noordhuis, A. Prabhu, S. J. Witte, A. Y. Chen, F. Cruz and C. Weniger, *Novel Constraints on Axions Produced in Pulsar Polar-Cap Cascades*, *Phys. Rev. Lett.* **131** (2023) 111004 [[2209.09917](#)].
- [144] D. Noordhuis, A. Prabhu, C. Weniger and S. J. Witte, *Axion Clouds around Neutron Stars*, [2307.11811](#).
- [145] W. H. Press and S. A. Teukolsky, *Floating Orbits, Superradiant Scattering and the Black-hole Bomb*, *Nature* **238** (1972) 211.
- [146] R. Brito, V. Cardoso and P. Pani, *Superradiance: New Frontiers in Black Hole Physics*, *Lect. Notes Phys.* **906** (2015) pp.1 [[1501.06570](#)].
- [147] P. B. Ferraz, T. W. Kephart and J. a. G. Rosa, *Superradiant pion clouds around primordial black holes*, *JCAP* **07** (2022) 026 [[2004.11303](#)].
- [148] N. Bernal, Y. F. Perez-Gonzalez and Y. Xu, *Superradiant production of heavy dark matter from primordial black holes*, *Phys. Rev. D* **106** (2022) 015020 [[2205.11522](#)].
- [149] D. Baumann, H. S. Chia and R. A. Porto, *Probing Ultralight Bosons with Binary Black Holes*, *Phys. Rev. D* **99** (2019) 044001 [[1804.03208](#)].
- [150] D. Levkov, A. Panin and I. Tkachev, *Gravitational Bose-Einstein condensation in the kinetic regime*, *Phys. Rev. Lett.* **121** (2018) 151301 [[1804.05857](#)].
- [151] J. Chen, X. Du, E. W. Lentz, D. J. E. Marsh and J. C. Niemeyer, *New insights into the formation and growth of boson stars in dark matter halos*, *Phys. Rev. D* **104** (2021) 083022 [[2011.01333](#)].

- [152] K. Kirkpatrick, A. E. Mirasola and C. Prescod-Weinstein, *Relaxation times for Bose-Einstein condensation in axion miniclusters*, *Phys. Rev. D* **102** (2020) 103012 [[2007.07438](#)].
- [153] J. Chen, X. Du, E. W. Lentz and D. J. E. Marsh, *Relaxation times for Bose-Einstein condensation by self-interaction and gravity*, *Phys. Rev. D* **106** (2022) 023009 [[2109.11474](#)].
- [154] K. Kirkpatrick, A. E. Mirasola and C. Prescod-Weinstein, *Analysis of Bose-Einstein condensation times for self-interacting scalar dark matter*, *Phys. Rev. D* **106** (2022) 043512 [[2110.08921](#)].
- [155] A. S. Dmitriev, D. G. Levkov, A. G. Panin and I. I. Tkachev, *Self-similar growth of Bose stars*, [2305.01005](#).
- [156] M. Jain, W. Wanichwecharungruang and J. Thomas, *Kinetic relaxation and nucleation of Bose stars in self-interacting wave dark matter*, [2310.00058](#).
- [157] G. B. Gelmini, *The Hunt for Dark Matter*, in *Theoretical Advanced Study Institute in Elementary Particle Physics: Journeys Through the Precision Frontier: Amplitudes for Colliders*, pp. 559–616, 2015, [1502.01320](#), DOI.
- [158] A. Maselli, P. Pnigouras, N. G. Nielsen, C. Kouvaris and K. D. Kokkotas, *Dark stars: gravitational and electromagnetic observables*, *Phys. Rev. D* **96** (2017) 023005 [[1704.07286](#)].
- [159] B. B. Kamenetskaia, A. Brenner, A. Ibarra and C. Kouvaris, *Proton capture in compact dark stars and observable implications*, *JCAP* **10** (2023) 027 [[2211.05845](#)].
- [160] D. Curtin and J. Setford, *How To Discover Mirror Stars*, *Phys. Lett. B* **804** (2020) 135391 [[1909.04071](#)].
- [161] M. Hippert, J. Setford, H. Tan, D. Curtin, J. Noronha-Hostler and N. Yunes, *Mirror neutron stars*, *Phys. Rev. D* **106** (2022) 035025 [[2103.01965](#)].
- [162] M. Hippert, H. Tan, J. Noronha-Hostler, N. Yunes, J. Setford and D. Curtin, *Mirror Neutron Stars: How QCD Can Be Used to Study Dark Matter Through Gravitational Waves*, *Acta Phys. Polon. Supp.* **16** (2023) 1 [[2207.13063](#)].
- [163] A. Mirizzi, G. G. Raffelt and P. D. Serpico, *Photon-axion conversion in intergalactic magnetic fields and cosmological consequences*, *Lect. Notes Phys.* **741** (2008) 115 [[astro-ph/0607415](#)].
- [164] R. Beck, *Galactic and Extragalactic Magnetic Fields*, *AIP Conf. Proc.* **1085** (2009) 83 [[0810.2923](#)].
- [165] G. Raffelt and L. Stodolsky, *Mixing of the Photon with Low Mass Particles*, *Phys. Rev. D* **37** (1988) 1237.
- [166] A. Cooray, *Extragalactic Background Light: Measurements and Applications*, [1602.03512](#).
- [167] NuSTAR collaboration, F. A. Harrison et al., *The Nuclear Spectroscopic Telescope Array (NuSTAR) High-Energy X-Ray Mission*, *Astrophys. J.* **770** (2013) 103 [[1301.7307](#)].
- [168] B. M. Roach, S. Rossland, K. C. Y. Ng, K. Perez, J. F. Beacom, B. W. Grefenstette et al., *Long-exposure NuSTAR constraints on decaying dark matter in the Galactic halo*, *Phys. Rev. D* **107** (2023) 023009 [[2207.04572](#)].
- [169] J. W. Foster, M. Kongsore, C. Dessert, Y. Park, N. L. Rodd, K. Cranmer et al., *Deep Search for Decaying Dark Matter with XMM-Newton Blank-Sky Observations*, *Phys. Rev. Lett.* **127** (2021) 051101 [[2102.02207](#)].

- [170] L. Bouchet, E. Jourdain, J. P. Roques, A. Strong, R. Diehl, F. Lebrun et al., *INTEGRAL SPI All-Sky View in Soft Gamma Rays: Study of Point Source and Galactic Diffuse Emissions*, *Astrophys. J.* **679** (2008) 1315 [[0801.2086](#)].
- [171] J. G. Stacy, W. Collmar, A. Strong, V. Schonfelder and A. Carraminana, *Limits on MeV Gamma-Ray Emission from Active Galaxies and Other Unidentified High-Latitude Gamma-Ray Sources Observed with COMPTEL*, in *International Cosmic Ray Conference*, vol. 3 of *International Cosmic Ray Conference*, pp. 1085–1088, Jan., 2008.
- [172] A. Strong and W. Collmar, *COMPTEL Reloaded: a heritage project in MeV astronomy*, *Mem. Soc. Ast. It.* **90** (2019) 297 [[1907.07454](#)].
- [173] A. W. Strong, I. V. Moskalenko and O. Reimer, *Diffuse galactic continuum gamma rays. A Model compatible with EGRET data and cosmic-ray measurements*, *Astrophys. J.* **613** (2004) 962 [[astro-ph/0406254](#)].
- [174] FERMI-LAT collaboration, M. Ackermann et al., *The spectrum of isotropic diffuse gamma-ray emission between 100 MeV and 820 GeV*, *Astrophys. J.* **799** (2015) 86 [[1410.3696](#)].
- [175] FERMI-LAT collaboration, G. Principe, *The Fermi Gamma Ray Sky: summary of recent Observations*, 9, 2022, [2209.03652](#).
- [176] LSST collaboration, J. A. Tyson, *Large synoptic survey telescope: Overview*, *Proc. SPIE Int. Soc. Opt. Eng.* **4836** (2002) 10 [[astro-ph/0302102](#)].
- [177] Y.-Y. Mao et al., *Snowmass2021: Vera C. Rubin Observatory as a Flagship Dark Matter Experiment*, [2203.07252](#).
- [178] T. Bessho, Y. Ikeda and W. Yin, *Indirect detection of eV dark matter via infrared spectroscopy*, *Phys. Rev. D* **106** (2022) 095025 [[2208.05975](#)].
- [179] J. P. Gardner et al., *The James Webb Space Telescope Mission*, *Publ. Astron. Soc. Pac* **135** (2023) 068001 [[2304.04869](#)].
- [180] R. Janish and E. Pinetti, *Hunting Dark Matter Lines in the Infrared Background with the James Webb Space Telescope*, [2310.15395](#).
- [181] S. Roy, C. Blanco, C. Dessert, A. Prabhu and T. Temim, *Sensitivity of JWST to eV-Scale Decaying Axion Dark Matter*, [2311.04987](#).
- [182] XRISM SCIENCE TEAM collaboration, *Science with the X-ray Imaging and Spectroscopy Mission (XRISM)*, [2003.04962](#).
- [183] A. Weltman et al., *Fundamental physics with the Square Kilometre Array*, *Publ. Astron. Soc. Austral.* **37** (2020) e002 [[1810.02680](#)].
- [184] R. Braun, A. Bonaldi, T. Bourke, E. Keane and J. Wagg, *Anticipated Performance of the Square Kilometre Array – Phase 1 (SKA1)*, [1912.12699](#).
- [185] O. Ghosh, J. Salvado and J. Miralda-Escudé, *Axion Gegenschein: Probing Back-scattering of Astrophysical Radio Sources Induced by Dark Matter*, [2008.02729](#).
- [186] D. Cadamuro and J. Redondo, *Cosmological bounds on pseudo Nambu-Goldstone bosons*, *JCAP* **02** (2012) 032 [[1110.2895](#)].
- [187] P. Carena, G. Lucente and E. Vitagliano, *Probing the blue axion with cosmic optical background anisotropies*, *Phys. Rev. D* **107** (2023) 083032 [[2301.06560](#)].

- [188] D. Grin, G. Covone, J.-P. Kneib, M. Kamionkowski, A. Blain and E. Jullo, *A Telescope Search for Decaying Relic Axions*, *Phys. Rev. D* **75** (2007) 105018 [[astro-ph/0611502](#)].
- [189] E. Todarello, M. Regis, J. Reynoso-Cordova, M. Taoso, D. Vaz, J. Brinchmann et al., *Robust bounds on ALP dark matter from dwarf spheroidal galaxies in the optical MUSE-Faint survey*, [2307.07403](#).
- [190] J. W. Foster, S. J. Witte, M. Lawson, T. Linden, V. Gajjar, C. Weniger et al., *Extraterrestrial Axion Search with the Breakthrough Listen Galactic Center Survey*, *Phys. Rev. Lett.* **129** (2022) 251102 [[2202.08274](#)].
- [191] ADMX collaboration, N. Du et al., *A Search for Invisible Axion Dark Matter with the Axion Dark Matter Experiment*, *Phys. Rev. Lett.* **120** (2018) 151301 [[1804.05750](#)].
- [192] ADMX collaboration, C. Boutan et al., *Piezoelectrically Tuned Multimode Cavity Search for Axion Dark Matter*, *Phys. Rev. Lett.* **121** (2018) 261302 [[1901.00920](#)].
- [193] ADMX collaboration, T. Braine et al., *Extended Search for the Invisible Axion with the Axion Dark Matter Experiment*, *Phys. Rev. Lett.* **124** (2020) 101303 [[1910.08638](#)].
- [194] N. Crisosto, P. Sikivie, N. S. Sullivan, D. B. Tanner, J. Yang and G. Rybka, *ADMX SLIC: Results from a Superconducting LC Circuit Investigating Cold Axions*, *Phys. Rev. Lett.* **124** (2020) 241101 [[1911.05772](#)].
- [195] ADMX collaboration, C. Bartram et al., *Dark matter axion search using a Josephson Traveling wave parametric amplifier*, *Rev. Sci. Instrum.* **94** (2023) 044703 [[2110.10262](#)].
- [196] ADMX collaboration, C. Bartram et al., *Search for Invisible Axion Dark Matter in the 3.3–4.2 μeV Mass Range*, *Phys. Rev. Lett.* **127** (2021) 261803 [[2110.06096](#)].
- [197] S. Lee, S. Ahn, J. Choi, B. R. Ko and Y. K. Semertzidis, *Axion Dark Matter Search around 6.7 μeV* , *Phys. Rev. Lett.* **124** (2020) 101802 [[2001.05102](#)].
- [198] J. Jeong, S. Youn, S. Bae, J. Kim, T. Seong, J. E. Kim et al., *Search for Invisible Axion Dark Matter with a Multiple-Cell Haloscope*, *Phys. Rev. Lett.* **125** (2020) 221302 [[2008.10141](#)].
- [199] CAPP collaboration, O. Kwon et al., *First Results from an Axion Haloscope at CAPP around 10.7 μeV* , *Phys. Rev. Lett.* **126** (2021) 191802 [[2012.10764](#)].
- [200] Y. Lee, B. Yang, H. Yoon, M. Ahn, H. Park, B. Min et al., *Searching for Invisible Axion Dark Matter with an 18 T Magnet Haloscope*, *Phys. Rev. Lett.* **128** (2022) 241805 [[2206.08845](#)].
- [201] J. Kim et al., *Near-Quantum-Noise Axion Dark Matter Search at CAPP around 9.5 μeV* , *Phys. Rev. Lett.* **130** (2023) 091602 [[2207.13597](#)].
- [202] A. K. Yi et al., *Axion Dark Matter Search around 4.55 μeV with Dine-Fischler-Srednicki-Zhitnitskii Sensitivity*, *Phys. Rev. Lett.* **130** (2023) 071002 [[2210.10961](#)].
- [203] B. Yang, H. Yoon, M. Ahn, Y. Lee and J. Yoo, *Extended Axion Dark Matter Search Using the CAPP18T Haloscope*, *Phys. Rev. Lett.* **131** (2023) 081801 [[2308.09077](#)].
- [204] C. M. Adair et al., *Search for Dark Matter Axions with CAST-CAPP*, *Nature Commun.* **13** (2022) 6180 [[2211.02902](#)].
- [205] CAST collaboration, A. A. Melcón et al., *First results of the CAST-RADES haloscope search for axions at 34.67 μeV* , *JHEP* **21** (2020) 075 [[2104.13798](#)].

- [206] T. Grenet, R. Ballou, Q. Basto, K. Martineau, P. Perrier, P. Pugnât et al., *The Grenoble Axion Haloscope platform (GrAHal): development plan and first results*, [2110.14406](#).
- [207] S. DePanfilis, A. C. Melissinos, B. E. Moskowitz, J. T. Rogers, Y. K. Semertzidis, W. U. Wuensch et al., *Limits on the abundance and coupling of cosmic axions at $4.5 < m_a < 5.0 \mu\text{eV}$* , *Phys. Rev. Lett.* **59** (1987) 839.
- [208] HAYSTAC collaboration, L. Zhong et al., *Results from phase 1 of the HAYSTAC microwave cavity axion experiment*, *Phys. Rev. D* **97** (2018) 092001 [[1803.03690](#)].
- [209] HAYSTAC collaboration, K. M. Backes et al., *A quantum-enhanced search for dark matter axions*, *Nature* **590** (2021) 238 [[2008.01853](#)].
- [210] HAYSTAC collaboration, M. J. Jewell et al., *New results from HAYSTAC's phase II operation with a squeezed state receiver*, *Phys. Rev. D* **107** (2023) 072007 [[2301.09721](#)].
- [211] D. Alesini et al., *Galactic axions search with a superconducting resonant cavity*, *Phys. Rev. D* **99** (2019) 101101 [[1903.06547](#)].
- [212] D. Alesini et al., *Search for invisible axion dark matter of mass $m_a = 43 \mu\text{eV}$ with the QUAX- $\alpha\gamma$ experiment*, *Phys. Rev. D* **103** (2021) 102004 [[2012.09498](#)].
- [213] D. Alesini et al., *Search for Galactic axions with a high-Q dielectric cavity*, *Phys. Rev. D* **106** (2022) 052007 [[2208.12670](#)].
- [214] B. T. McAllister, G. Flower, E. N. Ivanov, M. Goryachev, J. Bourhill and M. E. Tobar, *The ORGAN Experiment: An axion haloscope above 15 GHz*, *Phys. Dark Univ.* **18** (2017) 67 [[1706.00209](#)].
- [215] A. P. Quiskamp, B. T. McAllister, P. Altin, E. N. Ivanov, M. Goryachev and M. E. Tobar, *Direct search for dark matter axions excluding ALPogenesis in the 63- to 67- μeV range with the ORGAN experiment*, *Sci. Adv.* **8** (2022) abq3765 [[2203.12152](#)].
- [216] TASEH collaboration, H. Chang et al., *First Results from the Taiwan Axion Search Experiment with a Haloscope at 19.6 μeV* , *Phys. Rev. Lett.* **129** (2022) 111802 [[2205.05574](#)].
- [217] E-ASTROGAM collaboration, M. Tavani et al., *Science with e-ASTROGAM: A space mission for MeV-GeV gamma-ray astrophysics*, *JHEAp* **19** (2018) 1 [[1711.01265](#)].
- [218] A. De Angelis, V. Tatischeff, A. Argan, S. Brandt, A. Bulgarelli, A. Bykov et al., *Gamma-ray astrophysics in the mev range: The astrogam concept and beyond*, *Experimental Astronomy* **51** (2021) 1225–1254.
- [219] C. A. Kierans, *AMEGO: exploring the extreme multimessenger universe*, in *Space Telescopes and Instrumentation 2020: Ultraviolet to Gamma Ray* (J.-W. A. den Herder, S. Nikzad and K. Nakazawa, eds.), vol. 11444 of *Society of Photo-Optical Instrumentation Engineers (SPIE) Conference Series*, p. 1144431, Dec., 2020, [2101.03105](#), DOI.
- [220] K. Engel et al., *The Future of Gamma-Ray Experiments in the MeV-EeV Range*, in *Snowmass 2021*, 3, 2022, [2203.07360](#).
- [221] R. H. Dicke, *The Measurement of Thermal Radiation at Microwave Frequencies*, *Rev. Sci. Instrum.* **17** (1946) 268.
- [222] C. Ajello, G. Bonelli and G. Sironi, *Evaluation of earth's atmospheric brightness temperature at decimetric wavelengths*, *The Astrophysical Journal Supplement Series* **96** (1995) 643.

- [223] C. O’Hare, “cajohare/axionlimits: Axionlimits.” <https://cajohare.github.io/AxionLimits/>, July, 2020. 10.5281/zenodo.3932430.
- [224] J. S. Reynés, J. H. Matthews, C. S. Reynolds, H. R. Russell, R. N. Smith and M. C. D. Marsh, *New constraints on light axion-like particles using Chandra transmission grating spectroscopy of the powerful cluster-hosted quasar H1821+643*, *Mon. Not. Roy. Astron. Soc.* **510** (2021) 1264 [2109.03261].
- [225] M. C. D. Marsh, H. R. Russell, A. C. Fabian, B. P. McNamara, P. Nulsen and C. S. Reynolds, *A New Bound on Axion-Like Particles*, *JCAP* **12** (2017) 036 [1703.07354].
- [226] C. S. Reynolds, M. C. D. Marsh, H. R. Russell, A. C. Fabian, R. Smith, F. Tombesi et al., *Astrophysical Limits on Very Light Axion-like Particles from Chandra Grating Spectroscopy of NGC 1275*, *Astrophys. J.* **890** (2020) 59 [1907.05475].
- [227] C. Dessert, J. W. Foster and B. R. Safdi, *X-ray Searches for Axions from Super Star Clusters*, *Phys. Rev. Lett.* **125** (2020) 261102 [2008.03305].
- [228] C. Dessert, D. Dunsy and B. R. Safdi, *Upper limit on the axion-photon coupling from magnetic white dwarf polarization*, *Phys. Rev. D* **105** (2022) 103034 [2203.04319].
- [229] CAST collaboration, S. Andriamonje et al., *An Improved limit on the axion-photon coupling from the CAST experiment*, *JCAP* **04** (2007) 010 [hep-ex/0702006].
- [230] CAST collaboration, V. Anastassopoulos et al., *New CAST Limit on the Axion-Photon Interaction*, *Nature Phys.* **13** (2017) 584 [1705.02290].
- [231] S. Hoof and L. Schulz, *Updated constraints on axion-like particles from temporal information in supernova SN1987A gamma-ray data*, *JCAP* **03** (2023) 054 [2212.09764].
- [232] A. V. Gramolin, D. Aybas, D. Johnson, J. Adam and A. O. Sushkov, *Search for axion-like dark matter with ferromagnets*, *Nature Phys.* **17** (2021) 79 [2003.03348].
- [233] C. P. Salemi et al., *Search for Low-Mass Axion Dark Matter with ABRACADABRA-10 cm*, *Phys. Rev. Lett.* **127** (2021) 081801 [2102.06722].
- [234] M. Altmann, Y. Declais, F. v. Feilitzsch, C. Hagner, E. Kajfasz and L. Oberauer, *Search for the electron-positron decay of axions and axionlike particles at a nuclear power reactor at bugey*, *Zeitschrift für Physik C Particles and Fields* **68** (1995) 221.
- [235] G. Lucente and P. Carena, *Supernova bound on axionlike particles coupled with electrons*, *Phys. Rev. D* **104** (2021) 103007 [2107.12393].
- [236] M. Bauer, M. Neubert and A. Thamm, *Collider Probes of Axion-Like Particles*, *JHEP* **12** (2017) 044 [1708.00443].
- [237] F. Capozzi and G. Raffelt, *Axion and neutrino bounds improved with new calibrations of the tip of the red-giant branch using geometric distance determinations*, *Phys. Rev. D* **102** (2020) 083007 [2007.03694].
- [238] P. De la Torre Luque, S. Balaji and P. Carena, *Robust constraints on feebly interacting particles using XMM-Newton*, **2307.13728**.
- [239] P. De la Torre Luque, S. Balaji and P. Carena, *Multimessenger search for electrophilic feebly interacting particles from supernovae*, **2307.13731**.

- [240] M. Cirelli, E. Moulin, P. Panci, P. D. Serpico and A. Viana, *Gamma ray constraints on Decaying Dark Matter*, *Phys. Rev. D* **86** (2012) 083506 [[1205.5283](#)].
- [241] S. Ando and K. Ishiwata, *Constraints on decaying dark matter from the extragalactic gamma-ray background*, *JCAP* **05** (2015) 024 [[1502.02007](#)].
- [242] C. Blanco and D. Hooper, *Constraints on Decaying Dark Matter from the Isotropic Gamma-Ray Background*, *JCAP* **03** (2019) 019 [[1811.05988](#)].
- [243] S. L. Adler, *Placing direct limits on the mass of earth-bound dark matter*, *J. Phys. A* **41** (2008) 412002 [[0808.0899](#)].
- [244] N. P. Pitjev and E. V. Pitjeva, *Constraints on dark matter in the solar system*, *Astron. Lett.* **39** (2013) 141 [[1306.5534](#)].
- [245] XRISM SCIENCE TEAM collaboration, *XRISM Quick Reference*, [2202.05399](#).